AD-756 726

HELICOPTER BLADE FLUTTER

Norman D. Ham

Advisory Group for Aerospace Research and
Development
Paris, France

January 1973

AGARD

ADVISORY GROUP FOR AEROSPACE RESEARCH & DEVELOPMENT

7 RUE ANCELLE 92200 NEUILLY SUR SEINE FRANCE

AGARD REPORT No. 607

on

Helicopter Blade Flutter

by

N.D.Ham

D D C

RECEIVED

MAR 14 1973

B
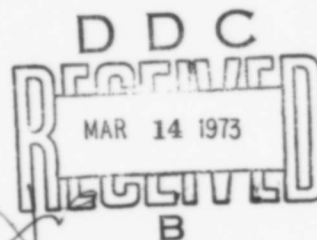
NORTH ATLANTIC TREATY ORGANIZATION

DISTRIBUTION AND AVAILABILITY
ON BACK COVER

NORTH ATLANTIC TREATY ORGANIZATION

ADVISORY GROUP FOR AEROSPACE RESEARCH AND DEVELOPMENT

(ORGANISATION DU TRAITE DE L'ATLANTIQUE NORD)

AGARD Report No.607

HELICOPTER BLADE FLUTTER

by

N.D.Ham

Massachusetts Institute of Technology
Cambridge, Mass. 02139, USA.

Revision of
Part III, Chapter 10
of the AGARD
MANUAL ON AEROELASTICITY

THE MISSION OF AGARD

The mission of AGARD is to bring together the leading personalities of the NATO nations in the fields of science and technology relating to aerospace for the following purposes:

- Exchanging of scientific and technical information;

- Continuously stimulating advances in the aerospace sciences relevant to strengthening the common defence posture;

- Improving the co-operation among member nations in aerospace research and development;

- Providing scientific and technical advice and assistance to the North Atlantic Military Committee in the field of aerospace research and development;

- Rendering scientific and technical assistance, as requested, to other NATO bodies and to member nations in connection with research and development problems in the aerospace field;

- Providing assistance to member nations for the purpose of increasing their scientific and technical potential;

- Recommending effective ways for the member nations to use their research and development capabilities for the common benefit of the NATO community.

The highest authority within AGARD is the National Delegates Board consisting of officially appointed senior representatives from each member nation. The mission of AGARD is carried out through the Panels which are composed of experts appointed by the National Delegates, the Consultant and Exchange Program and the Aerospace Applications Studies Program. The results of AGARD work are reported to the member nations and the NATO Authorities through the AGARD series of publications of which this is one.

Participation in AGARD activities is by invitation only and is normally limited to citizens of the NATO nations.

NORTH ATLANTIC TREATY ORGANIZATION

ADVISORY GROUP FOR AEROSPACE RESEARCH AND DEVELOPMENT

(ORGANISATION DU TRAITE DE L'ATLANTIQUE NORD)

ERRATA

AGARD Conference Proceedings No.80

**SYMPOSIUM ON UNSTEADY AERODYNAMICS FOR AEROELASTIC ANALYSIS OF
INTERFERING SURFACES, PART II**

Paper 12 UNSTEADY AERODYNAMICS FOR WINGS WITH CONTROL SURFACES by H.Tijdeman and
R.J.Zwaan.

1. Page 12-2 Section 2-2, 4th paragraph, 3rd line; add after ".... inboard control surface":

$$\text{"(AR} = 1.53, \ \Lambda_{LF} = 50.1°, \ t = 0.25, \ l_{tip}/l_{root} = 0.573 \ (\text{Ref.12}))."$$

2. substitute the reverse of this sheet for page 12-8.

12-8

Im(ΔCp)

7   T.E.

L.E.

5

4

3

Re(ΔCp)

2   T.E.

0   L.E.

Fig.6   Unsteady pressure distribution on a swept tapered wing with inboard
control surface at $M_\infty = 0.8$ and 120 Hz

| ○ MEASURED |
| — CALCULATED |
| $M_\infty = 0.5$ |
| $k = 1.036$ |

Im(ΔCp)

7   T.E.

L.E.

5

4

3

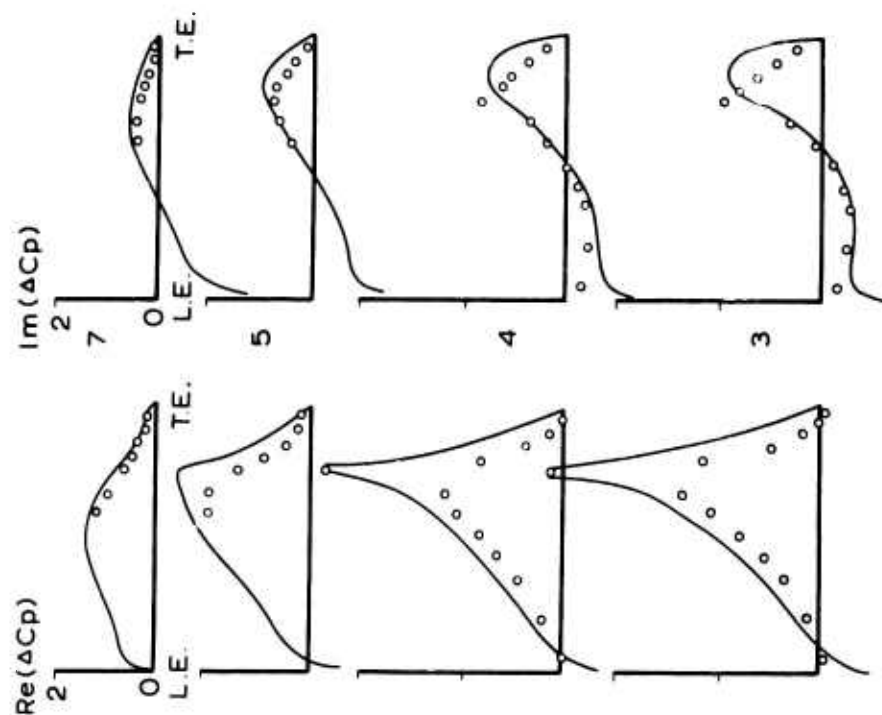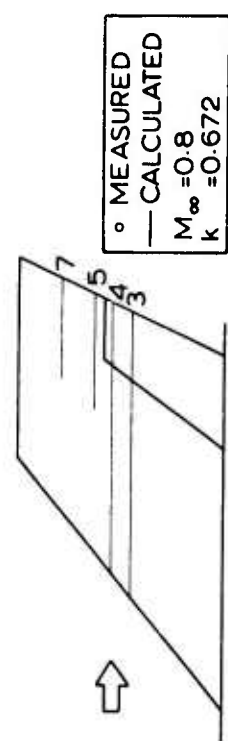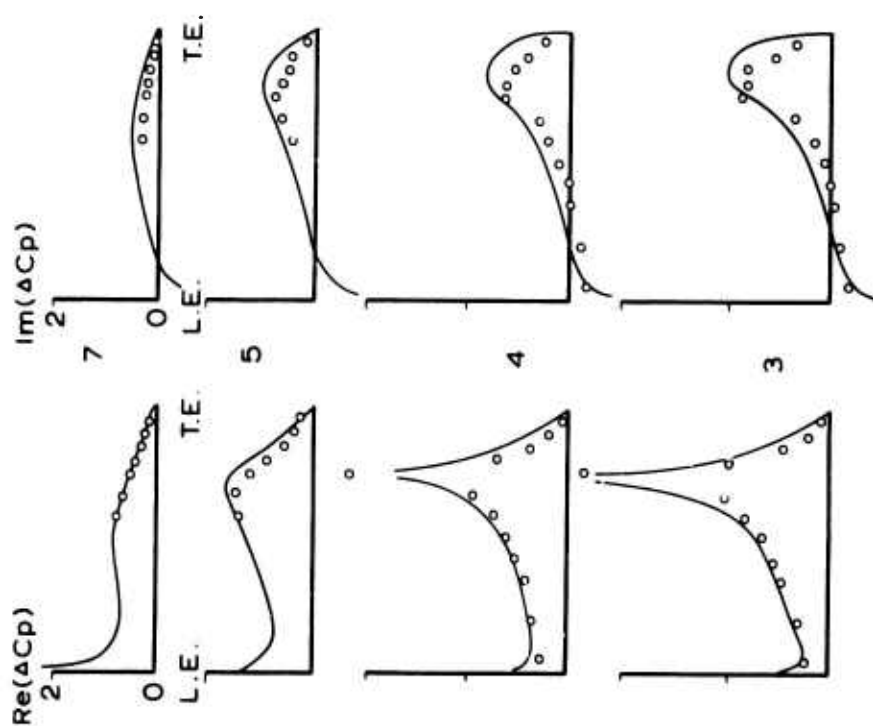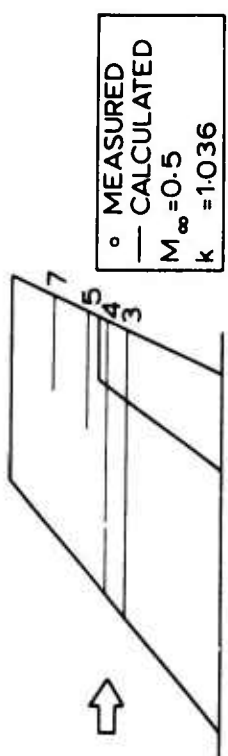Re(ΔCp)

2   T.E.

0   L.E.

Fig.5   Unsteady pressure distribution on a swept tapered wing with inboard
control surface at $M_\infty = 0.5$ and 120 Hz

PREFACE

Professor Norman D.Ham is presenting here a revised and up-dated version of the article he wrote in 1967, under the same title, for the Aeroelasticity Manual, and which was included in Chapter 10 of Volume III the following year.

Since that date, many advances and developments have been made regarding the vibration theory of the rotating parts of helicopters, and the understanding of the instabilities created in flight by these vibrations. For the Manual to continue to fulfil its information mission, it had become necessary to bring it up-to-date. Professor Ham, who had been the first one to draw attention to developments in the field covered by his article, accepted this task himself; no one could have brought it to a more successful issue.

New questions have been raised and solved. The analytical methods used to convert in-flight vibrations into equations and to detect aeroelastic instabilities are presented for hinged and locked blades, for take-off or cruise flights. The reasons for such instabilities are considered in detail, and efficient means prescribed to avoid them. Besides conventional type flutter, a large section is devoted to stall flutter. The text is illustrated and completed by many diagrams giving the results of calculations carried out in the United States.

Considered from a general standpoint, this article which is intended to replace that of 1968, provides an excellent survey of the data available in 1972 on the vibratory stability in flight of helicopters, and should therefore prove extremely useful to helicopter engineers and manufacturers.

R. MAZET
General Editor of the
Manual on Aeroelasticity

PREFACE

Le Professeur Norman D.Ham présente ici une édition révisée et complétée de l'article rédigé par lui sous le même ti re en 1967 pour le Manuel d'Aéroélasticité et qui a pris place au Chapitre 10 du Volume III l'année suivante.

Depuis cette date, de nombreux progrès et développements avaient été apportés à la théorie des vibrations des organes tournants des hélicoptères et à la connaissance des instabilités auxquelles ces vibrations donnent naissance en vol. Pour que le Manuel continue de remplir la mission d'information qui lui a été assignée, il devenait nécessaire de procéder à une remise à jour. Le Professeur Ham, qui avait le premier signalé l'évolution des connaissances sur la matière de son article, a bien voulu assumer lui-même ce travail; nul ne pouvait mieux que lui le mener à bien.

Des questions nouvelles sont posées et résolues. Les méthodes analytiques permettant de mettre en équations les vibrations en vol et de déceler les instabilités aéroélastiques sont présentées pour des pales articulées ou encastrées, pour le vol au décollage ou en croisière. Les raisons de ces instabilités sont examinées en détail et des moyens efficaces sont préconisés pour les éviter. A côté des flottements de types classiques, une large place est fait au flottement de décrochage (stall flutter). De nombreux graphiques traduisant en courbes les résultats de calculs effectués aux USA illustrent et complètent le texte.

D'une façon générale, cet article, qui est destiné à se substituer à celui de 1968, est une excellente synthèse des connaissances disponibles en 1972 sur la stabilité vibratoire en vol des hélicoptères et doit rendre, à ce titre, d'utiles services aux constructeurs et aux ingénieurs spécialistes de ces appareils.

R. MAZET
Editeur Général du Manuel
d'Aéroélasticité

CONTENTS

HELICOPTER BLADE FLUTTER

by

Norman D. Ham
Professor
MIT
Cambridge, Mass. 02139
U.S.A.

SUMMARY

Methods of analysis of helicopter blade flutter for both hinged and hingeless blades are presented. The major types considered are bending-torsion flutter, flap-lag flutter, and stall flutter. Both hover and forward flight are considered. Means of avoiding flutter are described.

SYMBOLS

a	blade section lift curve slope, per radian
b	blade section semi-chord
c	blade section chord
$g(t)$	displacement of blade first elastic bending mode
$g_k(t)$	displacement of blade kth bending mode
k	blade section reduced frequency, $\dfrac{\omega b}{\Omega R(x + \mu \sin\psi)}$
$m(r)$	blade spanwise running mass, slugs per foot
x	blade nondimensional spanwise station
x_A	chordwise displacement of section aerodynamic center from elastic axis, positive forward
x_I	chordwise displacement of section center of gravity from elastic axis, positive forward
r or s	spanwise distance along blade from axis of rotation
z	vertical distance from rotor hub plane
$C'(k)$	lift deficiency function including blade wake effects
C_T	rotor thrust coefficient
E	blade bending modulus of elasticity
F	real part of lift deficiency function
G	imaginary part of lift deficiency function
I	blade section second moment of area, flatwise bending, <u>or</u> ratio I_θ / I_1
I_1	blade moment of inertia about flapping hinge
I_0	blade section moment of inertia about its center of gravity
I_x	nondimensional blade product of inertia about flapping and elastic axes
I_k	nondimensional generalized mass of kth bending mode
I_θ	blade section moment of inertia about its elastic axis
$M(r)$	blade bending moment at r
M_{A_f}	blade section aerodynamic moment about elastic axis
R	rotor radius
T	rotor thrust
α	blade section angle of attack
α_0	blade section mean angle of attack
β	displacement of blade rigid flapping mode
γ	blade mass constant, or Lock number, $\dfrac{\rho a c R^4}{I_1}$
$\eta(r)$	mode shape of blade first elastic bending mode
$\eta_k(r)$	mode shape of blade kth bending mode
μ	rotor advance ratio $V/\Omega R$

2

ν	nondimensional root of bending-torsion characteristic equation
ν_k	nondimensional rotating natural frequency, kth bending mode
ω	imaginary part of ν
ω_K	rotating natural frequency, kth bending mode
ω_0	nonrotating natural frequency of blade torsional motion
ρ	air density
σ	rotor solidity
θ	blade pitch angle
ζ_θ	damping coefficient of blade torsional motion, divided by the critical damping coefficient
Ω	rotor rotational speed, radians per second
ψ	rotor blade azimuth angle, zero when reference blade is downstream
$\Theta(x)$	fundamental torsion mode shape

1. INTRODUCTION

The flutter of helicopter blades can be classified under the following categories:

(1) Flutter of Hinged Blades
(2) Flutter of Hingeless Blades
(3) Stall Flutter

The analysis of case (1) differs from the classical analysis of the high aspect ratio wing due to several important factors. The high centrifugal force field experienced by the rotating blade provides fundamental bending and torsional stiffness effects and also important coupling effects under certain circumstances. Also, the presence of the returning wake beneath the rotor at low flight speeds leads to unsteady aerodynamic effects that are substantially different from those characteristic of fixed wings. Finally, the variable velocity field encountered by the blade in forward flight generates important time variations in the velocity- and amplitude-dependent restoring forces acting on the blade.

The flutter in case (2) is due to the coupling between blade flapwise and lagwise motion which may lead to instability at large blade-pitch settings. This instability can occur at any flight speed provided the damping of the chordwise motion is below a certain value.

The instability associated with case (3) is due to the adverse time phasing of the aerodynamic torsional moment resulting from the loss of blade bound vorticity during torsional motion at high angles of attack. The complex nature of the phenomenon precludes an analytical representation of the unsteady airloads at the present time, but the prediction of regions of instability is made possible by the application of experimental two-dimensional data.

A useful survey of the various instabilities of rotors is presented in Reference (1).

2. FLUTTER OF HINGED BLADES

a. Equations of Motion

Consider bending out of the plane of rotation of the flexible, untwisted, untapered rotating blade shown in Figure (1). The bending moment at r due to forces at s is

$$M(r) = \int_r^R \left[\frac{dT(s)}{ds} - \ddot{z}(s)\, m(s) \right](s-r)\, ds$$

$$- \int_r^R s\Omega^2 m(s)\left[z(s) - z(r) \right] ds$$

Differentiating twice with respect to r yields

$$\frac{d^2 M(r)}{dr^2} = \frac{dT(r)}{dr} - m(r)\ddot{z}(r) + \frac{d^2 z(r)}{dr^2}\int_r^R s\Omega^2 m(s)\, ds - \frac{dz(r)}{dr} r\Omega^2 m(r)$$

$$M(r) = EI(r) \frac{d^2 z}{dr^2}$$

$$\therefore \frac{d^2}{dr^2}\left[EI(r)\frac{d^2 z}{dr^2}\right] - \frac{d^2 z}{dr^2}\int_r^R m(s)\, s\Omega^2 ds + r\Omega^2 m(r)\frac{dz}{dr} + m(r)\ddot{z} = \frac{dT}{dr} \tag{1}$$

the differential equation for a beam bending in a centrifugal force field.

Assume a series solution in terms of normal bending modes,

$$z = \sum_{k=1}^{\infty} \eta_k(r)\, g_k(t) \tag{2}$$

For free vibration of the rotating beam, neglecting aerodynamic damping, $dT(r)/dr = 0$. Substituting Eq. (2) into Eq. (1)

$$\sum_{k=1}^{\infty}\left\{\left[\frac{d^2}{dr^2}\left(EI\frac{d^2\eta_k}{dr^2}\right) - \frac{d^2\eta_k}{dr^2}\int_r^R m(s)\, s\Omega^2 ds + r\, m(r)\, \Omega^2 \frac{d\eta_k}{dr}\right]g_k + m\eta_k \ddot{g}_k\right\} = 0$$

Assuming simple harmonic motion at the kth rotating undamped natural bending frequency

$$g_k = \bar{g}_k\, e^{i\nu_k \Omega t}$$

$$\ddot{g} = -\nu_k^2 \Omega^2 \bar{g}_k\, e^{i\nu_k \Omega t} = -\nu_k^2 \Omega^2 g_k$$

$$\therefore \quad [\quad]\, g_k = \nu_k^2 \Omega^2 m\eta_k\, g_k$$

Therefore, the bending equation of motion becomes

$$\sum_{k=1}^{\infty} m\nu_k^2 \Omega^2 \eta_k g_k + \sum_{k=1}^{\infty} m\eta_k \ddot{g}_k = \frac{dT}{dr}$$

As an approximation, assume that all blade torsional flexibility is concentrated at the root (often true due to control system flexibility: the general case of distributed torsion is discussed in Reference (2)). Then, for the geometry of Figure (2), the coupled blade bending-torsion equation of motion is

$$\sum_{k=1}^{\infty} m\eta_k \ddot{g}_k + \sum_{k=1}^{\infty} m\nu_k^2 \Omega^2 \eta_k g_k - mx_I\ddot{\theta} - mx_I\Omega^2\theta = \frac{dT}{dr} \tag{3}$$

Multiply all terms of Eq. (3) by η_k and integrate from 0 to R:

$$\therefore \quad M_k \ddot{g}_k + M_k \nu_k^2 \Omega^2 g_k - (\ddot{\theta} + \Omega^2\theta)\int_0^R m\eta_k x_I\, dr = \int_0^R \eta_k \frac{dT}{dr}\, dr \tag{4}$$

where

$$M_k = \int_0^R m\eta_k^2\, dr \qquad k = 1, 2, \ldots \infty$$

$$\int_0^R m\eta_j\eta_k\, dr = 0 \qquad j \neq k$$

due to the orthogonality of the η_k's.

In practice an adequate representation of the blade bending motion is often obtained in terms of the first two modes only. On this basis the bending motion of an articulated blade is described by

$$z = r\beta + \eta g \tag{5}$$

where r = rigid flapping mode
     η = first elastic mode

4

Then if $I_1 \equiv M_1$; $I_2 = M_2/I$; $I_x = (1/I_1)\int_0^R mn_k x_I \, dr$, Eqs. (4) become, after division by $I_1 \Omega^2$, and since $\nu_1 = 1$,

$$\frac{\ddot{\beta}}{\Omega^2} + \beta - I_x \frac{\ddot{\theta}}{\Omega^2} - I_x \theta = \frac{1}{I_1 \Omega^2} \int_0^R r \frac{dT}{dr} \, dr \tag{6}$$

$$I_2 \frac{\ddot{g}}{\Omega^2} + I_2 \nu_2^2 g - I_{x_2} \frac{\ddot{\theta}}{\Omega^2} - I_{x_2} \theta = \frac{1}{I_1 \Omega^2} \int_0^R \eta \frac{dT}{dr} \, dr \tag{7}$$

Now consider torsional motion of the blade shown in Figure (2). Taking moments about the elastic axis,

$$-\int_0^R m(\ddot{z} - x_I \ddot{\theta}) x_I \, dr + \int_0^R I_0 \ddot{\theta} \, dr + \int_0^R I_0 \Omega^2 \theta \, dr + I_\theta \omega_0^2 \theta$$

$$-\int_0^R rm\Omega^2 \frac{dz(o)}{dr} x_I \, dr - \int_0^R m x_I \Omega^2 (z - r \frac{dz(o)}{dr} - x_I \theta) \, dr = \frac{1}{I_1 \Omega^2} \int_0^R \frac{dM_{A_f}}{dr} \, dr$$

for small z and θ, and no lag hinge. The term $[I_0 + \int_0^R x_I^2 \, dm] \Omega^2 \theta$ is the well-known "propeller moment".

Substituting Eq. (5) and dividing by $I_1 \Omega^2$,

$$I \frac{\ddot{\theta}}{\Omega^2} + I(1 + \omega_0^2)\theta - I_x \frac{\ddot{\beta}}{\Omega^2} - I_x \beta - I_{x_2} g = \frac{1}{I_1 \Omega^2} \int_0^R \frac{dM_{A_f}}{dr} \, dr \tag{8}$$

The aerodynamic terms in Eqs. (6), (7), and (8) are now considered in detail.

From Reference (3), P. 272, for unit span of a thin airfoil oscillating in incompressible flow, and neglecting small unsteady effects due to the unsteady component of U_T, Reference (4),

$$\frac{dT}{dr} = -\frac{1}{8} \rho a c^2 \left[\ddot{z} + U_T \dot{\theta} - (x_A - 0.25c) \ddot{\theta} \right]$$

$$-\frac{1}{2} \rho a c U_T C'(k) \left[U_P + U_T \theta + (0.5c - x_A) \dot{\theta} \right]$$

$$\frac{dM_{A_f}}{dr} = \frac{1}{8} \rho a c^2 \left[(x_A - 0.25c) \ddot{z} - U_T \dot{\theta}(0.5c - x_A) - \frac{c^2}{32} \ddot{\theta} - (x_A - 0.25c)^2 \ddot{\theta} \right]$$

$$+ \frac{1}{2} \rho a c U_T x_A C'(k) \left[U_P + U_T \theta + (0.5c - x_A) \dot{\theta} \right]$$

where the blade incident free-stream velocity, including rotor rotational velocity, is

$$U_T = \Omega r + \mu \Omega R \sin\psi$$

and the unsteady flow perpendicular to the blade is

$$U_P = \dot{z} + \mu \Omega R \frac{dz}{dr} \cos\psi$$

The quantity $C'(k)$ is comparable to the classical Theodorsen function $C(k)$, but has important differences due to the unique characteristics of the rotor wake. Typical values

of C'(k) are shown in Figure (3), taken from Reference (5).

In the present analysis, the virtual mass terms proportional to $\ddot{z}$ and $\ddot{\theta}$ are neglected for simplicity. They can be included if desired by appropriate adjustment (usually of the order of a few per cent) of the values of the blade inertial constants.

The aerodynamic terms can be expressed as follows:

$$\frac{1}{I_1 \Omega^2} \int_0^R r \frac{dT}{dr}\, dr = -m_{\dot{\beta}/\Omega}\, \frac{\dot{\beta}}{\Omega} - m_2\, \frac{\dot{g}}{\Omega} - m_{\dot{\theta}/\Omega} - m_\theta\, \theta - m_\beta\, \beta - m_{g_2}\, g$$

where

$$m_{\dot{\beta}/\Omega} = \frac{\gamma}{8}\, \overline{C'(k)} \left[1 + \frac{4}{3}\, \mu \sin\psi \right]$$

$$m_2 = \frac{\gamma}{2}\, \overline{C'(k)} \left[\int_0^1 x^2\, \frac{\eta}{R}\, dx + \mu \sin\psi \int_0^1 x\, \frac{\eta}{R}\, dx \right]$$

$$m_{\dot{\theta}/\Omega} = \frac{\gamma}{24} \left[1 + \frac{3}{2}\, \mu \sin\psi \right] \left[\frac{c}{R} + 4 \left(0.5\, \frac{c}{R} - \frac{x_A}{R} \right) \overline{C'(k)} \right]$$

$$m_\theta = \frac{\gamma}{8}\, \overline{C'(k)} \left[(1 + \mu^2) + \frac{8}{3}\, \mu \sin\psi - \mu^2 \cos 2\psi \right]$$

$$m_\beta = \frac{\gamma}{2}\, \overline{C'(k)} \left[\frac{1}{3}\, \mu \cos\psi + \frac{1}{4}\, \mu^2 \sin 2\psi \right]$$

$$m_{g_2} = \frac{\gamma}{2}\, \overline{C'(k)} \left[\mu \cos\psi \int_0^1 x^2\, \frac{d}{dx} \left(\frac{\eta}{R} \right) dx + \frac{1}{2}\, \mu^2 \sin 2\psi \int_0^1 x\, \frac{d}{dx} \left(\frac{\eta}{R} \right) dx \right]$$

The $\dot{\theta}/\Omega$ term is normally neglected for $c \ll R$. The coefficient $\overline{C'(k)}$ is a mean value based on conditions at the blade three-quarter radius. Also

$$\frac{1}{I_1 \Omega^2} \int_0^R \eta \frac{dT}{dr}\, dr = -m_2\, \frac{\dot{\beta}}{\Omega} - m_{\dot{g}/\Omega}\, \frac{\dot{g}}{\Omega} - m_{\dot{\theta}_2/\Omega}\, \frac{\dot{\theta}}{\Omega} - m_{\theta_2}\, \theta - m_{\beta_2}\, \beta - m_g\, g$$

where

$$m_{\dot{g}/\Omega} = \frac{\gamma}{2}\, \overline{C'(k)} \left[\int_0^1 \left(\frac{\eta}{R} \right)^2 x\, dx + \mu \sin\psi \int_0^1 \left(\frac{\eta}{R} \right)^2 dx \right]$$

$$m_{\dot{\theta}_2/\Omega} = \frac{\gamma}{8} \left[\mu \sin\psi \right] \left[\frac{c}{R} + 4 \left(0.5\, \frac{c}{R} - \frac{x_A}{R} \right) \overline{C'(k)} \right] \int_0^1 \frac{\eta}{R}\, dx +$$

$$\frac{\gamma}{8}\, \frac{c}{R} \int_0^1 x\, \frac{\eta}{R}\, dx + \frac{\gamma}{2}\, \overline{C'(k)} \left[0.5\, \frac{c}{R} - \frac{x_A}{R} \right] \int_0^1 x\, \frac{\eta}{R}\, dx$$

$$m_{\theta_2} = \frac{\gamma}{2}\, \overline{C'(k)} \left[\int_0^1 \left(\frac{\eta}{R} \right) x^2 dx + \mu^2 \sin^2\psi \int_0^1 \frac{\eta}{R}\, dx \right] + \gamma\, \overline{C'(k)}\, \mu \sin\psi \int_0^1 x\, \frac{\eta}{R}\, dx$$

$$m_{\beta_2} = \frac{\gamma}{2}\, \overline{C'(k)} \left[\frac{1}{2}\, \mu^2 \sin 2\psi \int_0^1 \frac{\eta}{R}\, dx + \mu \cos\psi \int_0^1 x\, \frac{\eta}{R}\, dx \right]$$

$$m_g = \frac{\gamma}{2}\, \overline{C'(k)} \left[\mu \cos\psi \int_0^1 x \left(\frac{\eta}{R} \right) \frac{d}{dx} \left(\frac{\eta}{R} \right) dx + \frac{1}{2}\, \mu^2 \sin 2\psi \int_0^1 \left(\frac{\eta}{R} \right) \frac{d}{dx} \left(\frac{\eta}{R} \right) dx \right]$$

Again, the $\dot{\theta}/\Omega$ term is neglected for $c \ll R$. Finally,

$$\frac{1}{I_1 \Omega^2} \int_0^R \frac{dM_{A_f}}{dr}\, dr = -M_{\dot{\theta}/\Omega}\, \frac{\dot{\theta}}{\Omega} - M_{\dot{\beta}/\Omega}\, \frac{\dot{\beta}}{\Omega} - M_{\dot{g}/\Omega}\, \frac{\dot{g}}{\Omega} - M_\beta\, \beta - M_\theta\, \theta - M_g\, g$$

6

where

$$M_{\dot\theta/\Omega} = \frac{\gamma}{8} \left[\frac{c}{R} - 4\overline{C'(k)} \frac{x_A}{R} \right] \left[0.5 \frac{c}{R} - \frac{x_A}{R} \right] \left[\frac{1}{2} + \mu \sin \psi \right]$$

$$M_{\dot\beta/\Omega} = -\frac{\gamma}{6} \frac{x_A}{R} \overline{C'(k)} \left[1 + \frac{3}{2} \mu \sin \psi \right]$$

$$M_{\dot g/\Omega} = -\frac{\gamma}{2} \frac{x_A}{R} \overline{C'(k)} \left[\int_0^1 x \frac{\eta}{R} dx + \mu \sin \psi \int_0^1 \frac{\eta}{R} dx \right]$$

$$M_\beta = -\frac{\gamma}{4} \frac{x_A}{R} \overline{C'(k)} \left[\mu \cos \psi + \mu^2 \sin 2\psi \right]$$

$$M_\theta = -\frac{\gamma}{6} \frac{x_A}{R} \overline{C'(k)} \left[1 + 3\mu \sin \psi + 3\mu^2 \sin^2 \psi \right]$$

$$M_g = -\frac{\gamma}{2} \frac{x_A}{R} \overline{C'(k)} \left[\mu \cos \psi \int_0^1 x \frac{d}{dx} \left(\frac{\eta}{R} \right) dx + \frac{1}{2} \mu^2 \sin 2\psi \int_0^1 \frac{d}{dx} \left(\frac{\eta}{R} \right) dx \right]$$

Note that in forward flight, when the flow direction reverses periodically with respect to portions of the blade, $x_A/R = 0.5$ c/R, and the blade damping in pitch $M_{\dot\theta/\Omega}$ becomes zero for such portions.

b. Method of Analysis

(1) In Hover

For discussion purposes, torsional motion θ and rigid flapping motion β of the rotating blade will be considered. Then the equations of motion become

$$\frac{\ddot\beta}{\Omega^2} + m_{\dot\beta/\Omega} \frac{\dot\beta}{\Omega} + (1 + m_\beta) \beta - I_x \frac{\ddot\theta}{\Omega^2} + (m_\theta - I_x) \theta = 0$$

$$-I_x \frac{\ddot\beta}{\Omega^2} + M_{\dot\beta/\Omega} \frac{\dot\beta}{\Omega} + (M_\beta - I_x) \beta + I \frac{\ddot\theta}{\Omega^2} + M_{\dot\theta/\Omega} \frac{\dot\theta}{\Omega} + \left[M_\theta + I + I \left(\frac{\omega_0}{\Omega} \right)^2 \right] \theta = 0$$

In hover, these equations have constant coefficients and can be solved by conventional techniques. Assuming simple harmonic motion, where

$$\beta = \overline{\beta} e^{\nu\Omega t}$$

$$\theta = \overline{\theta} e^{\nu\Omega t}$$

the characteristic equation of the motion is

$$A\nu^4 + B\nu^3 + C\nu^2 + D\nu + E = 0$$

For the case of quasi-static airloading, $\overline{C'(k)} = 1$, all coefficients of the characteristic equation are real, and the stability of disturbed motion can be evaluated using Routh's criteria.

When rotor wake effects are included, $\overline{C'(k)}$ is complex and a function of ν, and a trial and error solution is necessary. For the case of neutral stability, $\nu = i\omega$, where ω is the flutter frequency, and the characteristic equation can be separated into its real and imaginary components,

$$A'\omega^4 + B'\omega^3 + C'\omega^2 + D'\omega + E' = 0$$

$$A''\omega^4 + B''\omega^3 + C''\omega^2 + D''\omega + E'' = 0$$

where the coefficients are functions of ω. The pair of equations can then be solved simultaneously by assuming values of ω and solving each of the two equations for the parameter $(\omega_0/\Omega)^2$. Values of ω which yield identical values of this parameter for the two equations are the flutter frequencies ω_F, and the torsional stiffness or rotational speed at flutter is defined by the corresponding value of ω_0/Ω. Conditions for torsional divergence are not dependent on wake effects since for divergence $\omega = 0$.

The flutter and divergence boundaries for a hovering rotor were computed in Reference (6) for a rotor blade having the following properties:

$$\frac{\overline{C'(k)}}{\gamma} = \frac{1}{12}$$

$$I = .001$$
$$b/R = .05$$
$$x_A = 0$$

The results are presented in Figure (4).

The effect of the wake is shown in Figure (5) using values of $C'(k)$ from Reference (7) to recompute the hovering boundary of Figure (4). It is seen that neglecting the effect of the shed wake is adequate for design purposes in this instance.

The effect of blade flexibility on the flutter boundaries is also shown in Figure (5) by a single point computed for a blade bending frequency $v_2 = 2.5$. For conventional blades, neglect of bending flexibility results in negligible, though unconservative, error.

Further discussion and comparisons with test results are presented in References (8) and (9).

Usually flutter of conventional articulated helicopter blades is avoided by mass balancing them about the quarter-chord point, i e., by making the blade chordwise center-of-gravity position coincident with the blade section aerodynamic center. However, in certain instances appreciable blade bending coupled with a forward elastic axis location can lead to flutter even with mass balanced blades, References (8) and (10).

(ii) In Forward Flight

The equations of Section 2a can be solved numerically for the actual blade motion, including the forcing aerodynamic terms due to blade pitch angle, variable downwash, steady state flapping and bending, advancing blade Mach number, stall, and reverse flow.

A recent investigation, Reference 11, presents step-by-step computations of rotor blade motion, including the effect of blade dynamic stall, during flight at moderate to high advance ratios. The three degrees of freedom considered in the analysis are rigid blade pitching about the feathering axis, rigid blade flapping about the zero offset flapping hinge, and blade first mode flatwise elastic bending. Variable inflow and reverse flow are included in the computation of blade forces and moments. The calculation of inflow, aerodynamic loading, and blade motion is performed iteratively, using estimated steady state initial values.

Typical results are shown in Figures (6) and (7). The nature of these results suggests that classical methods of blade flutter and divergence analysis, carried over from fixed wing practice, should be replaced by numerical solution of the blade equations of motion including not only the conventional harmonic excitation forces, but also the nonlinear effects of reverse flow, variable inflow, dynamic stall, and compressibility.

Classical flutter is a highly periodic self-excited motion; rotor blade motion at high advance ratio is largely due to external excitation. The actual level of blade motion is the important criterion, as seen in the present results, which demonstrate not a stability boundary, but a blade stress level boundary due to the excited motion. Even the "classical flutter" case exhibits the effects of first harmonic excitation, while the "torsional divergence" case is the blade response to the lift acting at the blade three-quarter chord, and varying with the dynamic pressure over the reverse flow region.

At very high advance ratios, uncoupled flapping instability can occur due to negative aerodynamic damping and spring forces resulting from the periodic nature of the flow (Reference 12).

c. Finite Bending Effects

The preceding discussion has neglected the effect of steady state coning, collective pitch, and elastic bending displacement of the blade. For a conventional articulated rotor, these effects are small. However, for certain hub geometries, the steady state displacements of significant modes are of fundamental importance and cannot be neglected. A detailed analysis of such effects is presented in Reference (2). For example, in the absence of a lag hinge, steady state flatwise bending displacement of the blade introduces destabilizing moments due to centrifugal force which in extreme cases lead to instability when the blade chordwise center of gravity coincides with, or is even ahead of the blade aerodynamic center. These destabilizing moments are largely attenuated by the incorporation of a lag hinge.

3. FLUTTER OF HINGELESS BLADES

a. Equations of Motion

Classical blade flutter occurs due to the coupling of the torsional and flapping degrees of freedom. Under certain conditions, the two bending degrees of freedom of the blade (in the plane of rotation and out of the plane of rotation) couple together to produce another type of instability called flap-lag flutter.

In this section, the flap-lag-type instability of torsionally-rigid hingeless blades in the linear range of blade motion is treated in hover. This problem was first

treated by Young with a restrictive analytical approach (Reference 13). Modal equations of motion were obtained, but the numerical results were evaluated for a blade represented by a centrally-hinged, spring-restrained, equivalent model. Young concluded that the triggering mechanism of the flap-lag-type instability is the lag degree of freedom.

Hohenemser treated the same problem, using a somewhat unconventional numerical integration scheme (Reference 14). Due to the various approximations made in Reference 14, the results presented there are of a qualitative nature.

Consider the hingeless blade shown in the hub plane axis system of Figure (8). Following the analysis of Reference 15, the displacements v and w are expressed as

$$v/R = -\gamma_1(\bar{x}) h_1(t) \tag{1}$$

$$w/R = \eta_1(\bar{x}) g_1(t) \tag{2}$$

where $\eta_1(\bar{x})$ is the first normal mode shape of blade lapwise bending, and $g_1(t)$ is the modal displacement. Similarly, $\gamma_1(\bar{x})$ is the first normal mode shape for blade lagwise bending, and $h_1(t)$ is the modal displacement.

The nonlinear equation of motion for flapwise bending is shown in Reference 15 to be

$$\bar{M}_{F_1}(\overset{**}{g}_1 + \bar{\omega}_{F_1}^2 g_1) = 2\bar{P}_1 g_1 \overset{*}{h}_1 + \frac{\gamma}{2}\left[F_1\theta - F_2\lambda_0 - F_8\overset{*}{g}_1 - (2F_{10}\theta - F_{11}\lambda_0)\overset{*}{h}_1 + F_{13}\theta\overset{*}{h}_1^2 + F_{15}\overset{*}{g}_1\overset{*}{h}_1\right] \tag{3}$$

where
$$\bar{M}_{F_1} = \frac{R^3}{I_1}\int_0^1 m\eta_1^2\, d\bar{x}$$

$$\bar{\omega}_{F_1} = \text{first mode rotating flapping frequency}$$

$$\bar{P}_1 = \frac{R^3}{I_1}\int_0^1\left[\int_{\bar{x}}^1 m\gamma_1\, d\bar{x}_1\right](\eta_1')^2\, d\bar{x}$$

$$F_1 = \int_0^1 \bar{x}^2\eta_1\, d\bar{x} \qquad\qquad F_{10} = \int_0^1 \bar{x}\gamma_1\eta_1\, d\bar{x}$$

$$F_2 = \int_0^1 \bar{x}\eta_1\, d\bar{x} \qquad\qquad F_{11} = \int_0^1 \gamma_1\eta_1\, d\bar{x}$$

$$F_8 = \int_0^1 \bar{x}\eta_1^2\, d\bar{x}$$

$$\lambda_0 = \text{rotor inflow ratio referred to hub plane}$$

$$(\overset{*}{\ }) = d/d\psi \qquad\qquad (\ )' = d/dx$$

The nonlinear equation of motion for lagwise bending is shown in Reference 15 to be

$$\bar{M}_{L_1}(\overset{**}{h}_1 + \bar{\omega}_{L_1}^2 h_1) = (2\bar{S}_1 - 2\bar{M}_{\gamma_1}) h_1\overset{*}{h}_1 - 2\bar{M}_{\eta_1} g_1\overset{*}{g}_1$$

$$+ \frac{\gamma}{2}\left[(L_1\theta - L_2\lambda_0)\lambda_0 + \frac{C_{d_0}}{a}L_4\right.$$

$$+ (L_7\theta - 2L_8\lambda_0)\overset{*}{g}_1 - (L_{13}\theta\lambda_0 + 2\frac{C_{d_0}}{a}L_{14})\overset{*}{h}_1$$

$$\left. - L_{18}\overset{*}{g}_1^2 - L_{19}\theta\overset{*}{g}_1\overset{*}{h}_1\right] \tag{4}$$

where
$$\bar{M}_{L_1} = \frac{R^3}{I_1}\int_0^1 m\gamma_1^2\, d\bar{x}$$

$$\bar{\omega}_{L_1} = \text{first mode rotating lagging frequency}$$

$$\bar{S}_1 = \frac{R^3}{I_1} \int_0^1 (\gamma_1')^2 \left[\int_{\bar{x}}^1 m \, \gamma_1 \, d\bar{x}_1 \right] d\bar{x}$$

$$\bar{M}_{\eta_1} = \frac{R^3}{I_1} \int_0^1 m \, \gamma_1 \left[\int_0^{\bar{x}} (\eta_1')^2 d\bar{x}_1 \right] d\bar{x}$$

$$\bar{M}_{\gamma_1} = \frac{R^3}{I_1} \int_0^1 m \, \gamma_1 \left[\int_0^{\bar{x}} (\gamma_1')^2 d\bar{x} \right] d\bar{x}$$

C_{d_0} = blade section profile drag coefficient

$$L_1 = \int_0^1 \bar{x} \, \gamma_1 \, d\bar{x} \qquad\qquad L_{13} = \int_0^1 \gamma_1^2 \, d\bar{x}$$

$$L_2 = \int_0^1 \gamma_1 \, d\bar{x} \qquad\qquad L_{14} = \int_0^1 \bar{x} \, \gamma_1 \, d\bar{x}$$

$$L_4 = \int_0^1 \bar{x}^2 \gamma_1 \, d\bar{x} \qquad\qquad L_{18} = \int_0^1 \eta_1^2 \, \gamma_1 \, d\bar{x}$$

$$L_7 = \int_0^1 \bar{x} \, \eta_1 \gamma_1 \, d\bar{x} \qquad\qquad L_{19} = \int_0^1 \eta_1 \, \gamma_1^2 \, d\bar{x}$$

$$L_8 = \int_0^1 \eta_1 \gamma_1 \, d\bar{x}$$

Equations (3) and (4) are a system of two second order nonlinear equations describing the motion of the system. These equations are coupled through the following effects:

(a) Coriolis forces
(b) Shortening effects
(c) Aerodynamic forces

The nonlinear system given by Eqs. (3) and (4) are linearized about the static equilibrium condition (i.e., with all time derivatives set equal to zero), denoted by g_{1_0}, h_{1_0}; from the equations it is clear that

$$g_{1_0} = \frac{1}{\bar{M}_{F_1} \bar{\omega}_{F_1}^2} \frac{\gamma}{2} (F_1 \theta - F_2 \lambda_0) \tag{5}$$

$$h_{1_0} = \frac{1}{\bar{M}_{L_1} \bar{\omega}_{L_1}^2} \frac{\gamma}{2} \left[\lambda_0 (L_1 \theta - L_2 \lambda_0) + \frac{C_{d_0}}{a} L_4 \right] \tag{6}$$

Let

$$g_1 = g_{1_0} + \Delta g_1 \tag{7}$$

$$h_1 = h_{1_0} + \Delta h_1 \tag{8}$$

Substitution of Eqs. (7) and (8) into (3) and (4), and use of Eqs. (5) and (6) yields, after neglecting terms of type Δg_1^2, $\Delta g_1 \cdot \Delta h_1$, etc., and writing Δg_1, as g_1 for convenience,

$$\bar{M}_{F_1} (\ddot{g}_1 + \bar{\omega}_{F_1}^2 g_1) = 2\bar{P}_1 g_{1_0} \dot{g}_1 + \frac{\gamma}{2} \left\{ -\dot{g}_1 F_8 - (2F_{10}\theta - F_{11}\lambda_0)\dot{h}_1 \right\} \tag{9}$$

$$\bar{M}_{L_1} (\ddot{h}_1 + \bar{\omega}_{L_1}^2 h_1) = -2\bar{M}_{\eta_1} g_{1_0} \dot{g}_1 + \frac{\gamma}{2} \left\{ \dot{g}_1 (L_7 \theta - 2L_8 \lambda_0) - \dot{h}_1 \left[\lambda_0 \theta L_{13} + 2 \frac{C_{d_0}}{a} L_{14} \right] \right\} \tag{10}$$

Note that the term $2(\bar{S}_1 - \bar{M}_{\gamma_1})h_1\dot{h}_1 \simeq 0$ has been omitted in Eq. (10) because it is usually zero. For convenience, the following terms will be defined:

$$D_1 = \frac{\gamma}{2\bar{M}_{F_1}} F_8 \tag{11}$$

$$X = \left[2P_1 g_{1_0} - \frac{\gamma}{2} (2F_{10}\theta - F_{11}\lambda_0) \right] \frac{1}{\bar{M}_{F_1}} \tag{12}$$

$$D_2 = (\lambda_0 \theta L_{13} + 2 \frac{C_{d_0}}{\sigma} L_{14}) \frac{1}{\bar{M}_{L_1}} \qquad (13)$$

$$Y = -2 \bar{M}_{\eta_1} g_{1_0} + \frac{\gamma}{2} (L_7 \theta - 2 L_8 \lambda_0) \qquad (14)$$

With Eqs. (11) through (14), Eqs. (9) and (10) can be rewritten in the following convenient manner

$$\boxed{\begin{array}{l} \ddot{g}_1 + D_1 \dot{g}_1 + \bar{\omega}_{F1}^2 \, g_1 - X \dot{h}_1 = 0 \\ \ddot{h}_1 + D_2 \dot{h}_1 + \bar{\omega}_{L1}^2 \, h_1 - Y \dot{g}_1 = 0 \end{array}} \qquad (15)$$

From Eq. (15), it is clear that X,Y represent the coupling terms, and from Eqs. (12) and (14) it is clear that the coupling is partly due to Coriolis effects and partly due to aerodynamic effects.

The quantities D_1, D_2 represent the damping in the system, the damping inflap is a relatively large number, while the damping in lag is a small quantity of order C_{d_0}/a; the lag degree of freedom is the potentially unstable one.

b. Method of Analysis

The flutter or the critical condition of the linearized system (15) is characterized by the existence of a small amplitude oscillation for Eqs. (15).

Assume the solution in the form

$$g_1 = A_1 e^{p\psi} , \quad h_1 = A_2 e^{p\psi}$$

Substitution of these into (15) yields the following characteristic equation

$$(p^2 + D_1 p + \bar{\omega}_{F_1}^2)(p^2 + D_2 p + \bar{\omega}_{L_1}^2) - p^2 XY = 0 \qquad (16)$$

For a small value of θ, the root of Eq. (16) has Real(p) < 0 and the solution is stable. For $\theta = \theta_c$, the system is neutrally stable. For $\theta > \theta_c$, at least one of the roots of Eq. (16) has Real(p) > 0 and the system is unstable.

At $\theta = \theta_c$, there are two solutions to Eq. (16) such that p is imaginary:

$$p = \pm i\omega_c$$

Substituting into (16) and setting to zero the real and imaginary part of (16) yields

$$\omega_c^2 = \frac{D_1 \bar{\omega}_{L_1}^2 + D_2 \bar{\omega}_{F_1}^2}{D_1 + D_2} = \frac{\bar{\omega}_{L_1}^2 + \frac{D_2}{D_1} \bar{\omega}_{F_1}^2}{1 + \frac{D_2}{D_1}} \qquad (17)$$

$$(-\omega_c^2 + \bar{\omega}_{F_1}^2)(-\omega_c^2 + \bar{\omega}_{L_1}^2) - \omega_c^2 D_1 D_2 + \omega_c^2 X Y = 0 \qquad (18)$$

where ω_c is the flutter frequency. It is interesting to note that $D_2/D_1 \ll 1$. Therefore,

$$\omega_c^2 \simeq \bar{\omega}_{L1}^2$$

Stability boundaries resulting from the solution of Eqs. (17) and (18) are shown in Figure 9 for no structural damping and the mode shapes

$$\eta_1 = \gamma_1 = -\frac{1}{3} [1 - 4\bar{x} - (1 - \bar{x})^4]$$

The areas inside the elliptical boundaries are combinations of rotating flap and lag frequencies for which the system is unstable. These areas are reduced for increasing structural damping, and increased for increasing γ.

c. Torsional Effects

The addition of the torsional degree of freedom is stabilizing for the lower branch of the flap-lag stability boundary shown in Figure 9, and strongly destabilizing for the upper branch, as shown in Figure 10.

Note: Important effects are associated with the nonlinearities contained in Eqs. (3) and (4). For further details, see Reference (15).

4. STALL FLUTTER

    a. Aerodynamic Loading During Dynamic Stall

        Studies described in References (20) and (21) have shown that the negative damping
in pitch associated with airfoils oscillating at high mean angles of attack can lead to
torsional instability of helicopter rotor blades under certain conditions. The mechanism
of the instability was shown to consist of the adverse time phasing of the aerodynamic
pitching moment associated with the loss of blade bound vorticity as the dynamic stall
occurs.

        Subsequent tests, Reference (22), indicated that the same mechanism is found for
the case of airfoil linear angle-of-attack change through high angles of attack. The
nature of these results indicated several important conclusions not only with respect to
the analysis of rotor blade stall flutter instability, but also with respect to the gen-
eral nature of the aerodynamic loading of an airfoil experiencing transient angle-of-
attack changes of large magnitude.

        A typical time history of the pressure variation acting at one spanwise station
of a model helicopter rotor blade experiencing stall-induced oscillations while operating
in the static thrust condition showed the initiation of a pressure disturbance in the
region of the leading edge as the blade section approaches maximum angle of attack, and
the subsequent motion of this disturbance in the chordwise direction, at considerably less
than free-stream velocity. The character of the disturbance suggested that it consisted
of free vorticity introduced into the blade flow field from the neighborhood of the blade
leading edge during the dynamic stall process. The results indicated that the dynamic
stall phenomenon has far different characteristics than those associated with the static
stall of an airfoil.

        The negative pressure peak generated by the pressure disturbance moving aft from
the leading edge leads to a nose-down pitching moment component in phase with the nose-
down motion of the airfoil. Since this nose-down moment is generated once per pitching
cycle, it is seen that the nonlinear aerodynamic moment variation due to pitching motion
at high mean angles of attack is such as to sustain the motion. This self-excited, self-
limiting motion is termed "stall flutter".

        The above results suggested that the same stall mechanism would be found in the
general case of large transient blade angle-of-attack changes. Accordingly, an experi-
mental investigation was commenced at MIT to study large linear angle-of-attack changes
of a two-dimensional wing (Reference (22)). Comparison of the dynamic lift variation
with the corresponding values of static lift at the same angles of attack indicated that
the maximum dynamic lift achieved was substantially higher than the maximum static lift.
A very large, sustained, transient nose-down moment occurred in the high angle-of-attack
region.

        The origin of these effects was found in the corresponding chordwise pressure
variations. Dynamic stall began to occur, as indicated by the drop in leading-edge suc-
tion, at an angle of attack much higher than that for static stall. A negative pressure
disturbance moving aft from the leading edge simultaneously increased the suction in the
mid-chord region. Subsequently, the pressure disturbance moved further aft and was still
of considerable magnitude. The delay in the occurrence of stall (as evidenced by loss of
leading-edge suction) due to the high rate of change of angle of attack, and the sustained
upper surface suction associated with the chordwise passage of the vorticity shed during
the stall process, both contributed to the high sustained lift. In addition, the in-
creasingly aft center of pressure due to the aft motion of the shed vorticity generated
extreme nose-down pitching moment. Finally, the pressure distribution indicated greatly
increased pressure drag on the airfoil. This drag may be a transient analog of the
"vortex drag" due to the leading edge vortex of a slender delta wing at low speed and
high angle of attack.

        The above results led to several important conclusions with respect to stall
flutter and airload prediction of high speed and/or highly loaded helicopter rotor blades.

        1. The stall of an airfoil section during rapid transient high angle-of-
            attack changes is delayed well above the static stall angle and re-
            sults in a large transient negative pressure disturbance leading to
            large transient lift and nose-down pitching moment.

        2. The magnitude of the pitching moment of (1) is such as to generate
            substantial nose-down pitching displacements of the blade. These
            pitching displacements can substantially alter the angle-of-attack
            distribution of the rotor blade. Transient pitching displacement
            of the blade in response to the initial stall-induced pitching moment
            acting on the blade should be included in stall flutter analyses.

        3. The dynamic stall phenomenon of a helicopter rotor blade can be
            separated into three major phases:

            a. A delay in the loss of blade leading-edge suction to an angle
                of attack above the static stall angle, with associated airloads
                of the type described by classical unsteady airfoil theory.
            b. A subsequent loss of leading-edge suction accompanied by the
                formation of a large negative pressure disturbance (due to the
                shedding of vorticity from the vicinity of the blade leading

edge) which moves aft over the upper surface of the blade. Associated with this phase are high transient lift, drag, and nose-down pitching moment associated with the greatly altered pressure distribution on the airfoil.

c. Complete upper surface separation of the classic static type, characterized by low lift, high drag, and moderate nose-down pitching moment.

b. Method of Analysis

Investigations of harmonically oscillating two-dimensional wings in forced motion, for example, References (15), (16), (17), (18), (19), (20), and (21) have demonstrated that under stalled conditions the average damping in pitch over a cycle can become substantially negative and is strongly dependent on the wing mean angle of attack, the reduced frequency of the harmonic motion, the oscillation amplitude, and the airfoil configuration and pitch-axis location. Reference (16) indicated that the origin of the negative damping was aerodynamic moment hysteresis, and that for certain mean angles of attack, reduced frequencies and amplitudes of oscillation, the mean damping in pitch was zero over a cycle, and that, under these conditions, a self-excited but self-limiting one degree of freedom limit cycle oscillation of prescribed amplitude could occur. These results indicate that potential theory unsteady aerodynamic predictions of two-dimensional airfoil pitch damping are progressively less representative as the mean angle of attack approaches the static stalling angle. Typical variation of the pitch damping with mean angle of attack is shown in Figure (11). This figure represents an analytic synthesis of data presented in References (16), (17), and (20). In the referenced experiments, the amplitudes of the stable limit cycle oscillation were developed as functions of the initial angle of attack and reduced frequency. In the present analytic synthesis, an attempt was made to correct for differences in rotation point and static stalling angles of the various data. This was followed by a calculation of equivalent viscous damping. The necessary balance of energy over a cycle of oscillation yielded a generalized equivalent viscous pitch damping function. This equivalent viscous damping function by the nature of the averaging process smooths out the higher frequency components of the destabilizing aerodynamic pitching moment. It is important to note that the instantaneous values of negative damping vary about this mean value and can be substantially more negative near the stalling angle.

The extent of the stalled regions of a helicopter rotor and the possibilities for unstable pitching-torsional oscillations are illustrated in Figure (12) which illustrates a typical angle-of-attack distribution in the high speed cruise condition. This distribution is based on a detailed calculation of the rotor velocity field, and indicates an extensive region of stall; the corresponding net integrated pitch damping is found to be negative over a significant range of azimuth angles. This indicates the origin of a transiently unstable pitching-torsional oscillation which will occur with a once per rotor revolution repetition rate. Since only a few cycles of torsional motion are possible before the blade becomes unstalled, limit cycle motion is usually not achieved. However, substantial increases in blade torsional stress and pitch link loads are possible either by self-excitation or in response to external disturbances.

Experimental evidence of such unstable pitching-torsional oscillations or rotor blade "stall flutter" is abundant. The term "comfort stall" has been used to describe an almost asymptotic rise in cyclic pitch link loadings and related helicopter vibratory phenomena which occur when significant zones of blade stall are present. Some typical experimental evidence of this asymptotic rise in cyclic pitch link loadings is presented in Figure (13) in the form of a set of wave forms showing the time variation of the torsional loading in a typical case.

In view of the experimentally derived damping function, the current insight into the rotor stalling pattern, and this experimental evidence, it is evident that the net pitch damping of the rotor blade can and often does become periodically negative in forward flight. Therefore, whenever combinations of thrust ratio and rotor advance ratio result in significant zones of blade stall, an unstable torsional oscillation may result.

The stability boundary can be approximated by considering the net aerodynamic pitch damping of the rotor blade control system fundamental pitching-torsion mode of oscillation. Because of the complex angle-of-attack distributions which occur in forward flight, this net damping function will vary widely with azimuth. It can be expected to exhibit a heavily damped condition in the region of blade advance, and can be expected to exhibit a negatively damped condition in the region of blade retreat, if large values of rotor thrust coefficient-solidity ratio and/or rotor advance ratio lead to significant zones of stalling. Inasmuch as the instantaneous negative pitch damping can exceed the averages shown in Figure (11), a simple approximation of the stability boundary is obtained by the condition that the motion will be transiently unstable if

$$\left[\zeta_\theta(\psi)\right]_{\substack{\text{weighted}\\\text{average}}} \equiv \int_0^1 \Theta_1^2(x)\, \zeta_\theta\left[\alpha_0(x,\psi)\right]\, dx \leq 0$$

where the reduced frequency is based on the actual velocity at the reference radius of the retreating blade rather than on the mean velocity, i.e.:

$$k(x,\psi) = \frac{\omega_\theta b}{\Omega R(x+\mu \sin\psi)}$$

In other words, the local blade element average damping ratio (depending on the

local initial angle of attack and local reduced frequency) is weighted by the square of the local fundamental mode amplitude to obtain the net pitch damping at each azimuth angle. If this weighted average damping becomes negative at any azimuth angle, the pitching-torsional motion can be expected to become transiently unstable. If the range of azimuth angles over which the pitch damping is negative is broad enough to permit one or more cycles of a torsional oscillation, a marked increase in cyclic control loading can be expected.

To illustrate the application of this stability criterion, a calculation of the net damping function versus azimuth angle was carried out in Reference (20) for a severe rotor loading condition characterized by $\mu = .17$ and $C_m/\sigma = .111$. The result of this calculation is presented in dimensional form in Figure (14). It is seen that the net pitch damping is negative for the region bounded by the azimuth angles 225° and 10° (or 370°). Stall flutter would be expected to occur. Figure (13) presents torsional strain and pressure data for this flight condition which is seen to support the theoretical prediction of stall flutter. The trace of absolute pressure transducer at the 80 percent radius station and 5 percent chord point is indicative of the loss of leading edge suction and accompanying pitching moment variation. It is seen that the blade torsional response to this initially nose-down moment exhibits an unstable behavior in the region in which the net damping in pitch is negative. In this case, the instability is short-lived, but especially pronounced, as evidenced by the peak in the pitch link load trace near the 330° azimuth.

A more precise method of evaluating stall flutter effects has recently been developed (References (23), (24), (25), (26)). The equations of motion, e.g., Subsection 2a, are solved numerically for the actual blade motion, including the forcing aerodynamic terms due to blade dynamic stall.

The representation of blade dynamic stall is based on the results of References (22) and (27), some of which are presented in Figure (15). The applicability of these two-dimensional results to the rotating blade is demonstrated in Reference (28). It is seen that under conditions of rapid transient, as opposed to oscillatory, blade angle-of-attack change, the maximum lift and torsional moment generated are proportional to $\dot{\alpha}^{(s)}c/V$, where (s) denotes the value at the instant of dynamic stall, and are considerably larger in magnitude than those measured in tests of airfoils oscillating through the stall. In the latter case it is believed that some degree of flow separation persists throughout the oscillatory cycle, leading to forces and moments that are lower than those found in the transient tests.

The three degrees of freedom considered in the analysis are rigid blade pitching about the feathering axis, rigid blade flapping about the zero offset flapping hinge, and blade first mode flatwise elastic bending. Variable inflow and reverse flow are included in the computation of blade forces and moments. The calculation of inflow, aerodynamic loading, and blade motion is performed iteratively, using estimated steady-state initial values.

A typical result is shown in Figure (16). The corresponding rotor angle-of-attack distribution is shown in Figure (17). Note that the blade passes in and out of stall several times as a result of its torsional response to the initial dynamic stall.

c. Means of Alleviating Stall Flutter

Several approaches to the design problem of postponing rotor blade stall flutter are evident. The first is the obvious one of avoiding significant regions of blade stall by increasing rotor solidity beyond that dictated by ordinary performance considerations. This approach may incur a performance penalty. Excess solidity increases rotor profile drag, resulting in a reduced rotor lift to effective drag ratio at the design point, with an attendant loss in the helicopter's range and maximum speed capability. A second approach is to counteract the negative aerodynamic pitch damping with positive mechanical damping. The difficulty stems from the deformation pattern associated with the fundamental torsion mode. Generally, this mode is twisting motion in addition to rigid body pitching against the effective torsional spring of the helicopter control system. In this case, a dashpot in parallel with the control system is relatively ineffective, and internal torsional damping becomes necessary; this is slight in conventional metal rotor blade structures. On the other hand, the use of a glass fiber-resin matrix structure could be expected to dissipate considerable energy in torsion due to its visco-elastic damping which varies with the rate of shear strain.

The most appealing approach, with the least performance penalty and design complication is to reduce the extent of the stalled zones by departing from the typical contemporary blade airfoil section, and employing sections having high dynamic stall angles. Sections having an appreciable amount of leading edge camber have favorable dynamic stall characteristics (References (29) and (30)).

REFERENCES

1. Loewy, R.G., "Review of Rotary Wing V/STOL Dynamic and Aeroelastic Problems", Journal of the American Helicopter Society, 14, 3, July 1969.

2. Miller, R.H., and Ellis, C.W., "Blade Vibration and Flutter", *Journal of the American Helicopter Society*, 1, 3, July 1956.

3. Bisplinghoff, R.L., Ashley, H., and Halfman, R.L., *Aeroelasticity*, Addison Wesley, 1955.

4. Greenberg, J.M., *Airfoil in Sinusoidal Motion in a Pulsating Stream*, National Advisory Committee for Aeronautics Technical Note 1326, June 1947.

5. Miller, R.H., "Unsteady Air Loads on Helicopter Rotor Blades", *Journal of the Royal Aeronautical Society*, 68, 640, April 1964.

6. Miller, R.H., *Aeroelastic Problems of VTOL Aircraft*, Notes for a Special Summer Program, Aeroelastic and Structures Research Laboratory, M.I.T., June 1958.

7. Loewy, R.G., "A Two-Dimensional Approximation to the Unsteady Aerodynamics of Rotary Wings", *Journal of the Aeronautical Sciences*, 24, 2, February 1957.

8. Zvara, J., *The Aeroelastic Stability of Helicopter Rotors in Hovering Flight*, Aeroelastic and Structures Research Laboratory, M.I.T., Technical Report 61-1, September 1956.

9. Daughaday, H., DuWaldt, F., and Gates, C., "Investigation of Helicopter Blade Flutter and Load Amplification Problems", *Journal of the American Helicopter Society*, 2, 3, July 1957.

10. Sibley, J.D., and Jones, C.H., "Some Design Aspects of Tandem Rotor Helicopters", *Journal of the Helicopter Association of Great Britain*, 13, 5, October 1959.

11. Ham, N.D., and Johnson, W., "Comparison of Dynamically Scaled Model Rotor Test Data with Step-by-Step Calculations of Rotor Blade Motion", Paper No. 341A, *American Helicopter Society 25th Annual National Forum*, May 1969.

12. Perisho, C.H., "Analysis of the Stability of a Flexible Helicopter Blade at High Advance Ratio", *Journal of the American Helicopter Society*, 4, 2, April 1959.

13. Young, M.I., "A Theory of Rotor Blade Motion Stability in Powered Flight", *Journal of the American Helicopter Society*, 9, 3, July 1964.

14. Hohenemser, K.H., and Heaton, P.W., "Aeroelastic Instability of Torsionally Rigid Helicopter Blades", *Journal of the AHS*, 12, 2, April 1967.

15. Friedmann, P., and Tong, P., *Dynamic Nonlinear Elastic Stability of Helicopter Rotor Blades in Hover and in Forward Flight*, M.I.T. Aeroelastic and Structures Research Laboratory, ASRL TR 166-3, May 1972.

16. Halfman, R.L. et. al., *Evaluation of High-Angle-of-Attack Aerodynamic Derivative Data and Stall-Flutter Prediction Techniques*, NACA TN2533, 1951.

17. Rainey, A.G., *Preliminary Study of Some Factors which Affect the Stall-Flutter Characteristics of Thin Wings*, NACA TN3622, 1956.

18. Rainey, A.G., *Measurement of Aerodynamic Forces for Various Mean Angles of Attack on an Airfoil Oscillating in Pitch, etc., with Emphasis on Damping in the Stall*, NACA TR1305, 1957.

19. Bratt, J.B., and Wight, K.C., *The Effect of Mean Incidence, Amplitude of Oscillation, Profile and Aspect Ratio on Pitching Moment Derivatives*, Aeronautical Research Committee R. and M. No. 2064, 1945.

20. Ham, N.D., and Young, M.I., "Torsional Oscillation of Helicopter Blades Due to Stall", *Journal of Aircraft*, 3, 3, May-June 1966.

21. Carta, F.O., "An Analysis of the Stall Flutter Instability of Helicopter Rotor Blades", *Journal of the American Helicopter Society*, 12, 4, October 1967.

22. Ham, N.D., and Garelick, M.S., "Dynamic Stall Considerations in Helicopter Rotors", *Journal of the American Helicopter Society*, 13, 2, April 1968.

23. Johnson, W., "The Effect of Dynamic Stall on the Response and Airloading of Helicopter Rotor Blades", *Journal of the American Helicopter Society*, 14, 2, April 1969.

24. Gross, D.W., and Harris, F.D., "Prediction of Inflight Stalled Airloads from Oscillating Airfoil Data", Paper No. 322, *American Helicopter Society 25th Annual National Forum*, May 1969.

25. Tarzanin, F.J., "Prediction of Control Loads Due to Blade Stall", *Journal of the American Helicopter Society*, 17, 2, April 1972.

26. Carta, F.O., Commerford, G.L., and Carlson, R.G., "Determination of Airfoil and Rotor Blade Dynamic Stall Response", Preprint No. 613, *American Helicopter Society 28th Annual National Forum*, May 1972.

27. Ham, N.D., "Aerodynamic Loading on a Two-Dimensional Airfoil During Dynamic Stall", *AIAA Journal*, 6, 10, October 1968.

28. McCroskey, W.J., and Fisher, R.K., "Detailed Aerodynamic Measurements on a Model Rotor in the Blade Stall Regime", *Journal of the American Helicopter Society*, 17, 1, January 1972.

29. Liiva, J., and Davenport, F.J., "Dynamic Stall of Airfoil Sections for High-Speed Rotors", *Journal of the American Helicopter Society*, 14, 2, April 1969.

30. Benson, R.G., Dadone, L.U., Gormont, R.E., and Hohler, G.R., "Influence of Airfoils on Stall Flutter Boundaries of Articulated Helicopter Rotors", Preprint No. 621, *American Helicopter Society 28th Annual National Forum*, May 1972.
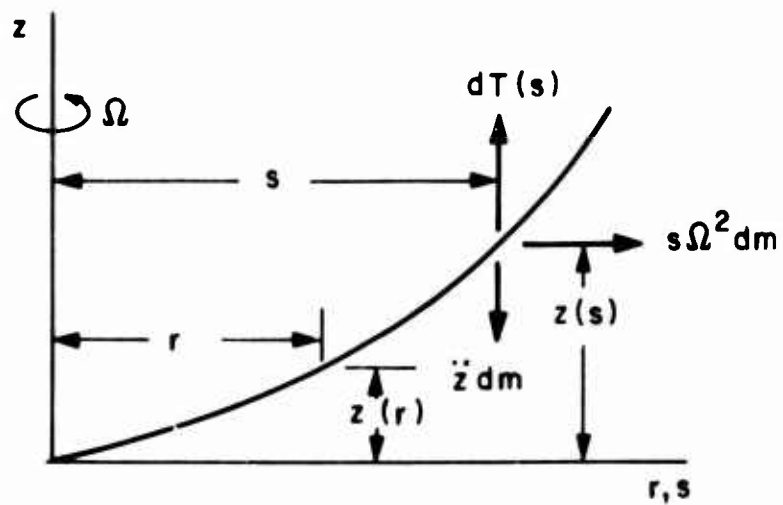
Fig.1   Blade bending geometry
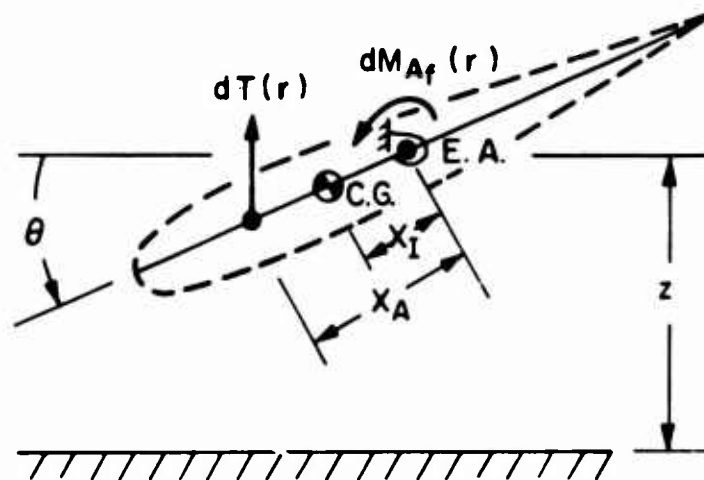
Fig.2   Blade torsional geometry
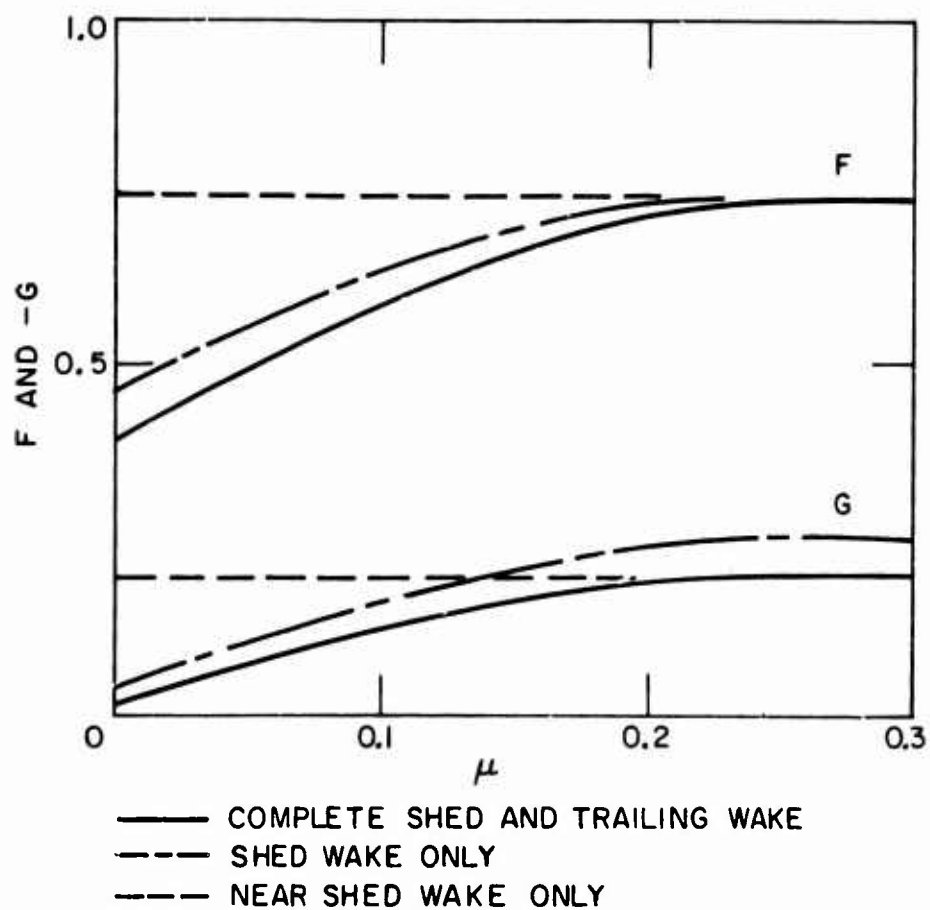
Fig.3   Effect of advance ratio μ on unsteady aerodynamic effects
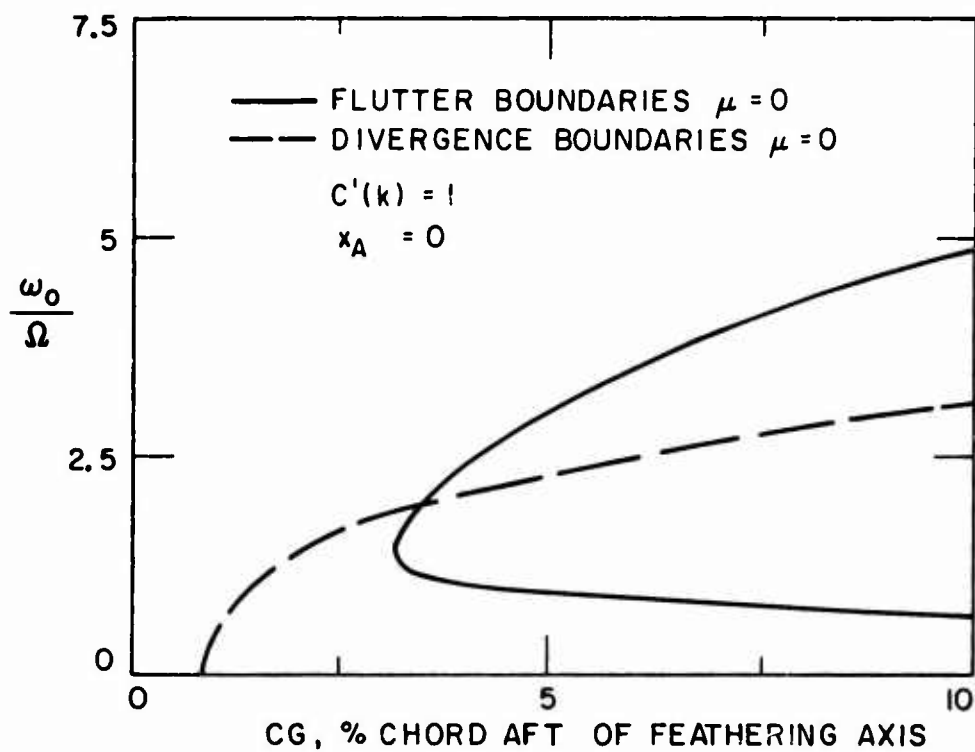
Fig.4   Flutter and divergence boundaries for flapping rotor blade
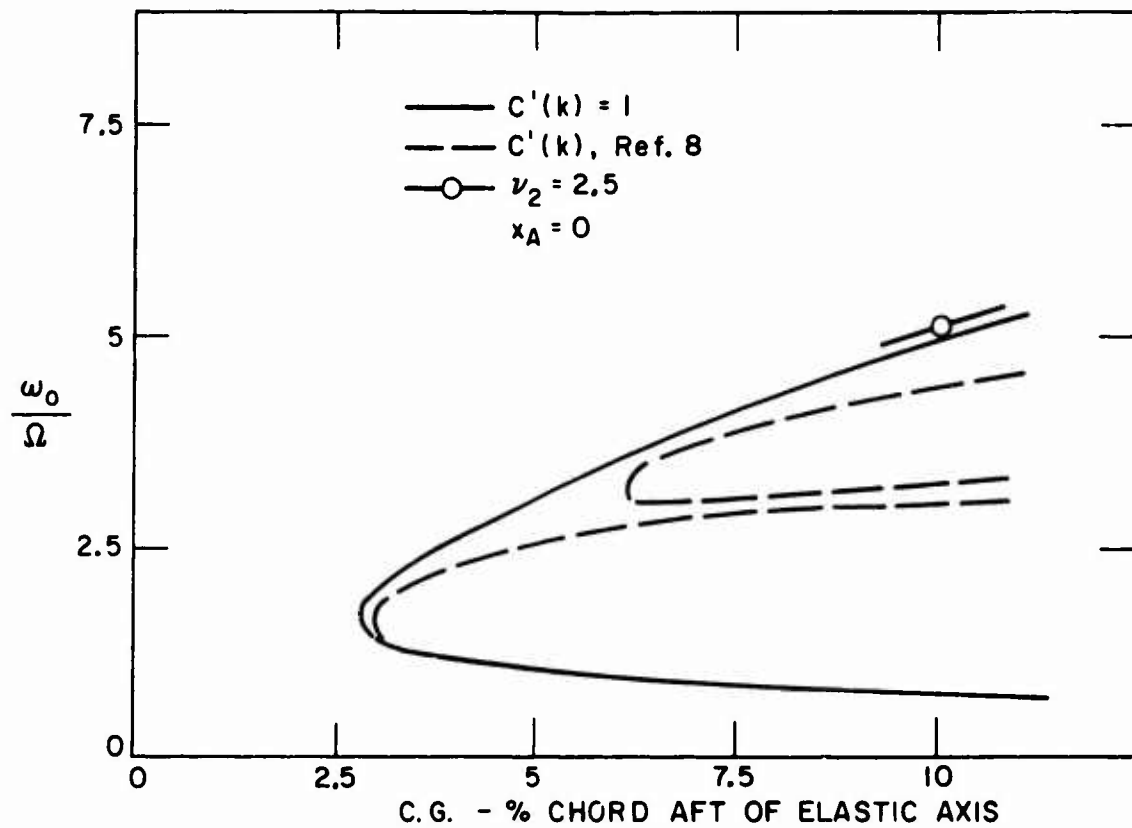
Fig.5   Flutter boundaries in hovering
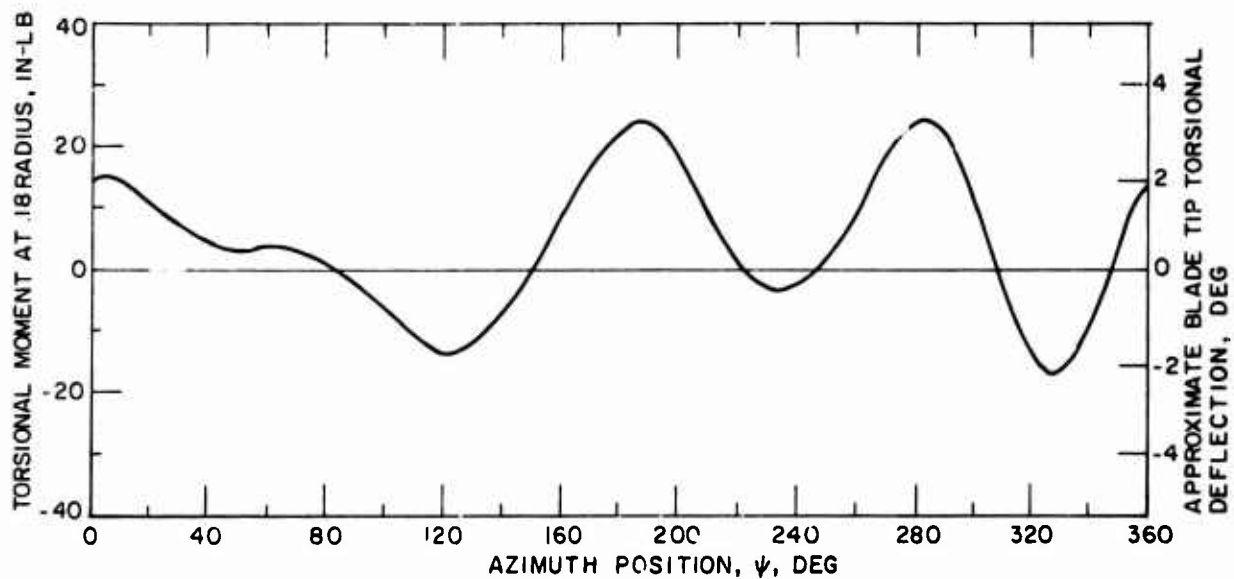
Fig.6   Blade response to classical flutter $\mu = .68$,   V = 284 knots, $\theta_0 = 4°$ blade C.G. at 30% chord
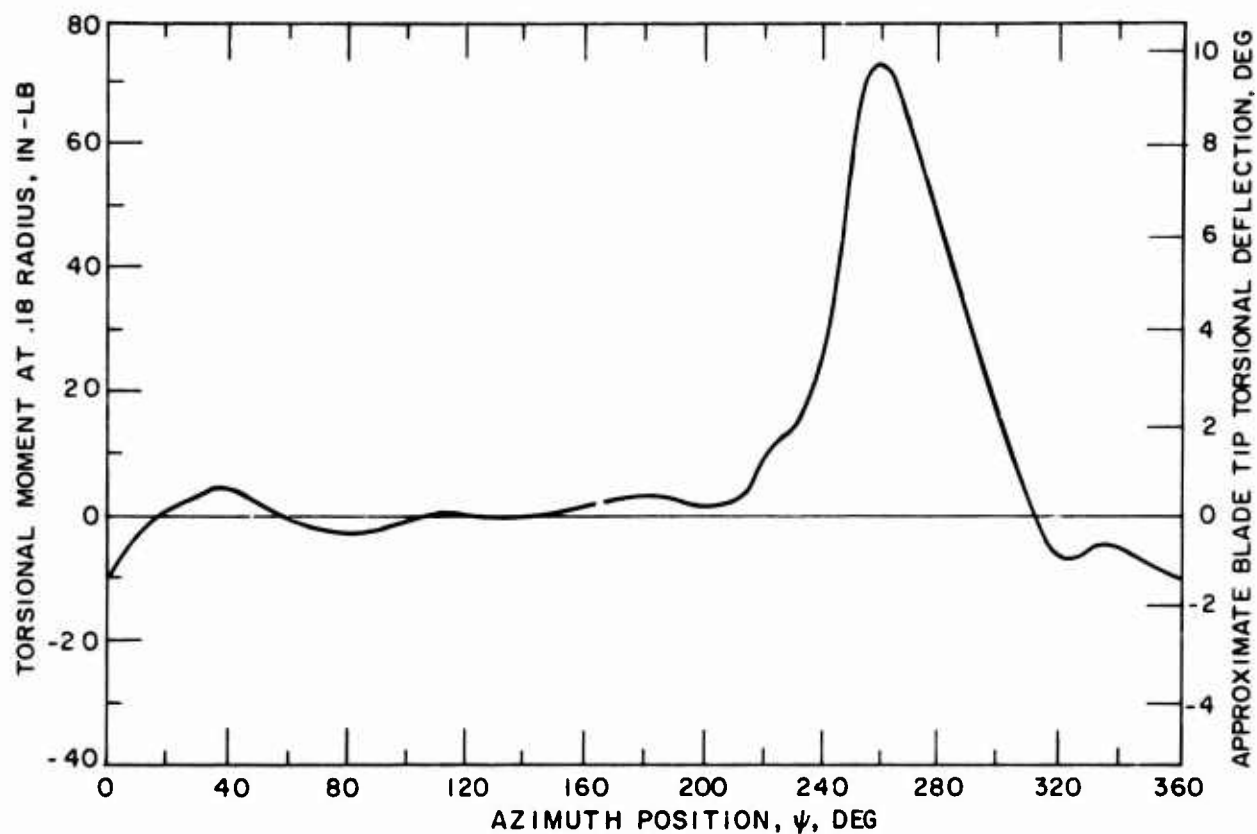
Fig.7   Blade response to torsional divergence. $\mu = 1.47$, $V = 332$ knots $\theta_0 = 2°$ blade C.G. at 25% chord
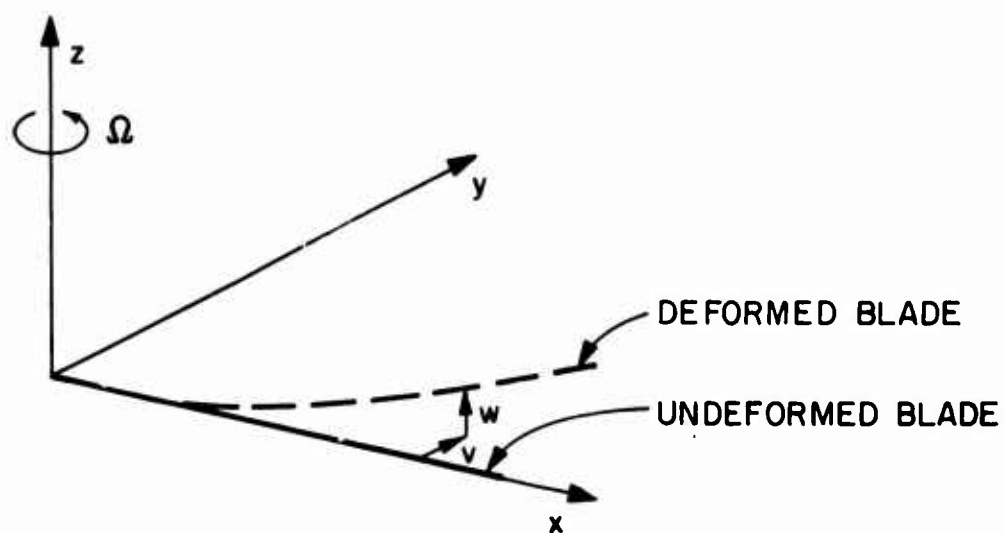
Fig.8   Geometry of undeformed blade and deformed blade
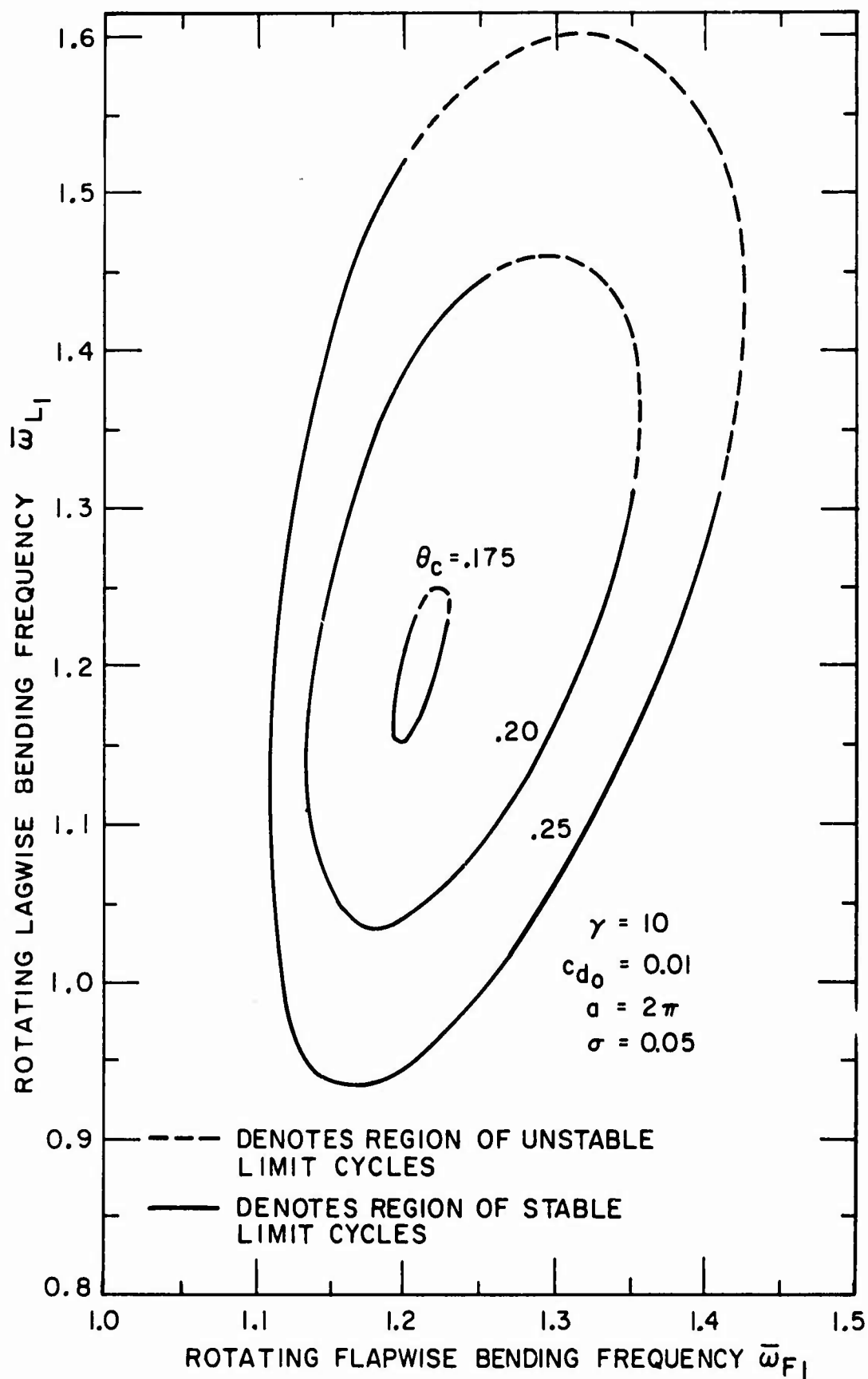
Fig.9 Stability boundaries for various values of θ_c
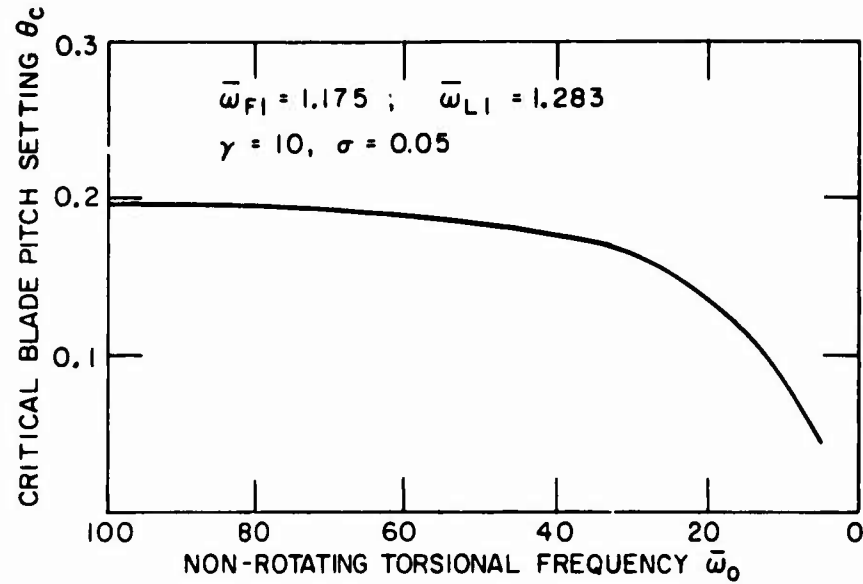
Fig.10   Effect of torsional degree of freedom on flap-lag type of instability
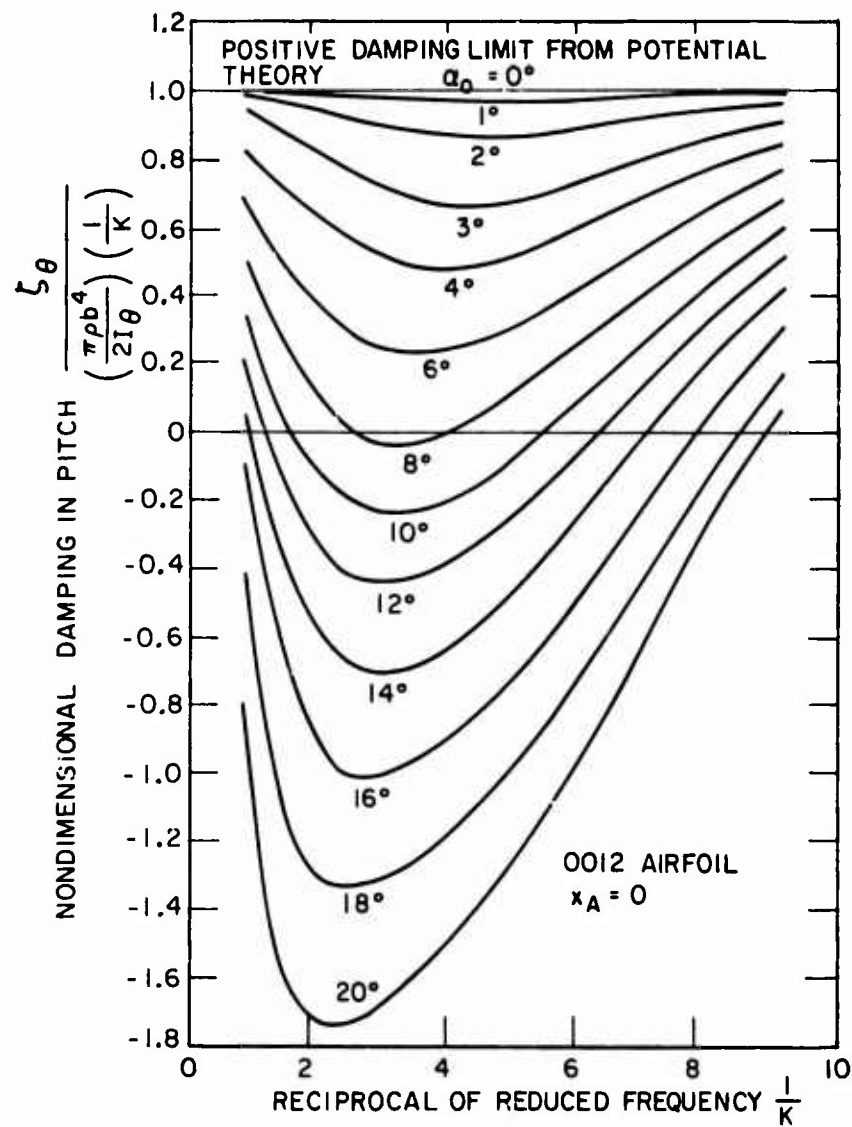
Fig.11   Approximation for generalized pitch damping
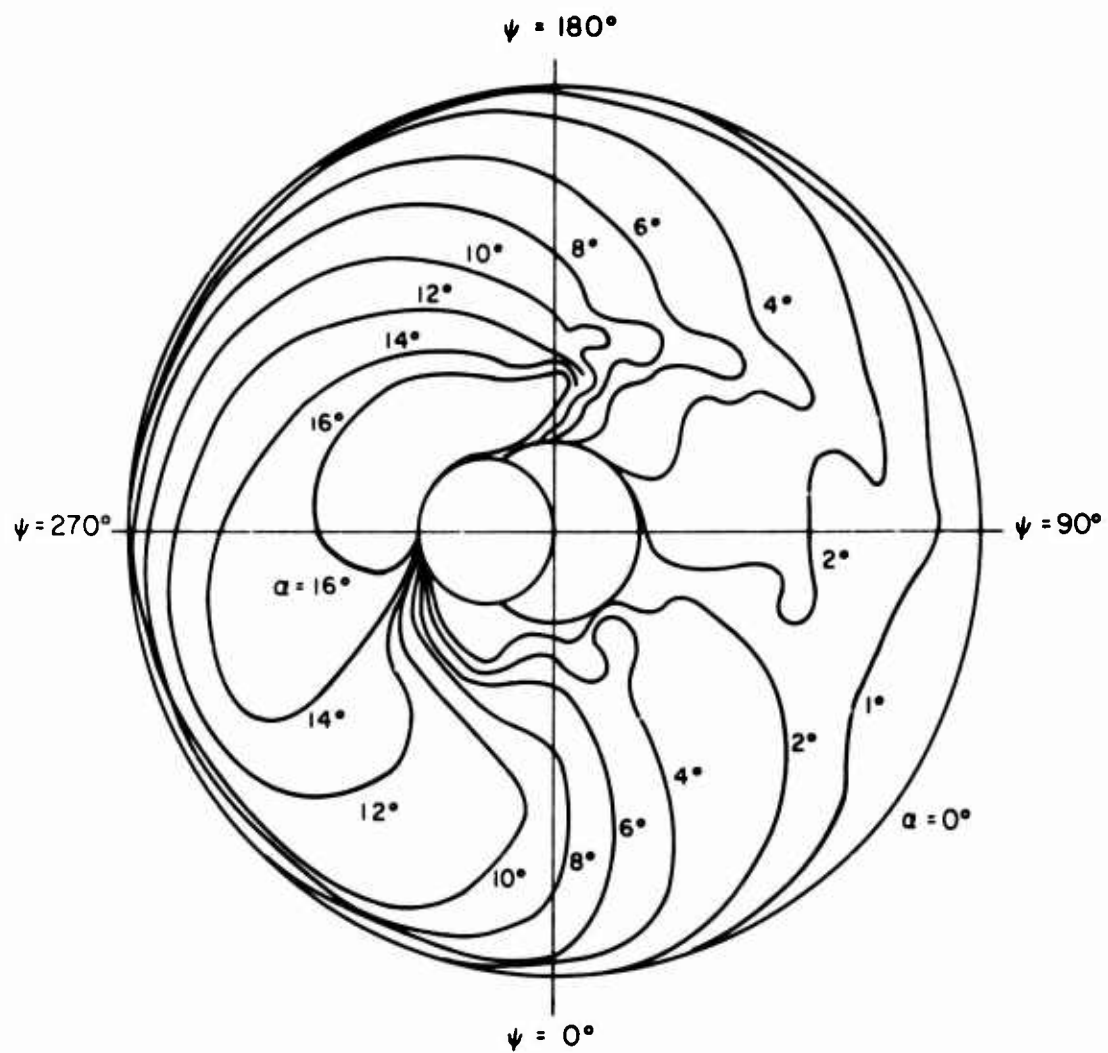
Fig.12 Theoretical angle of attack distribution — with non-uniform downwash; Vertol model CH-47A front rotor
V = 140 kts; forward C.G. position, gross weight = 27.500 lbs.

23
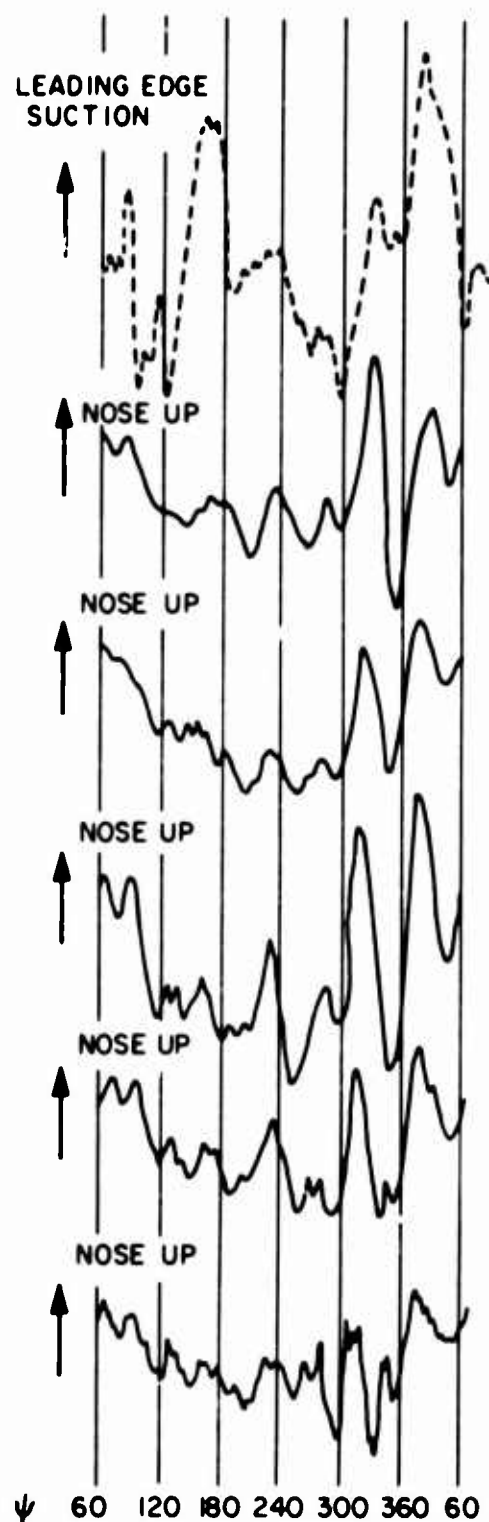
Fig.13   Airload and strain character of stall flutter
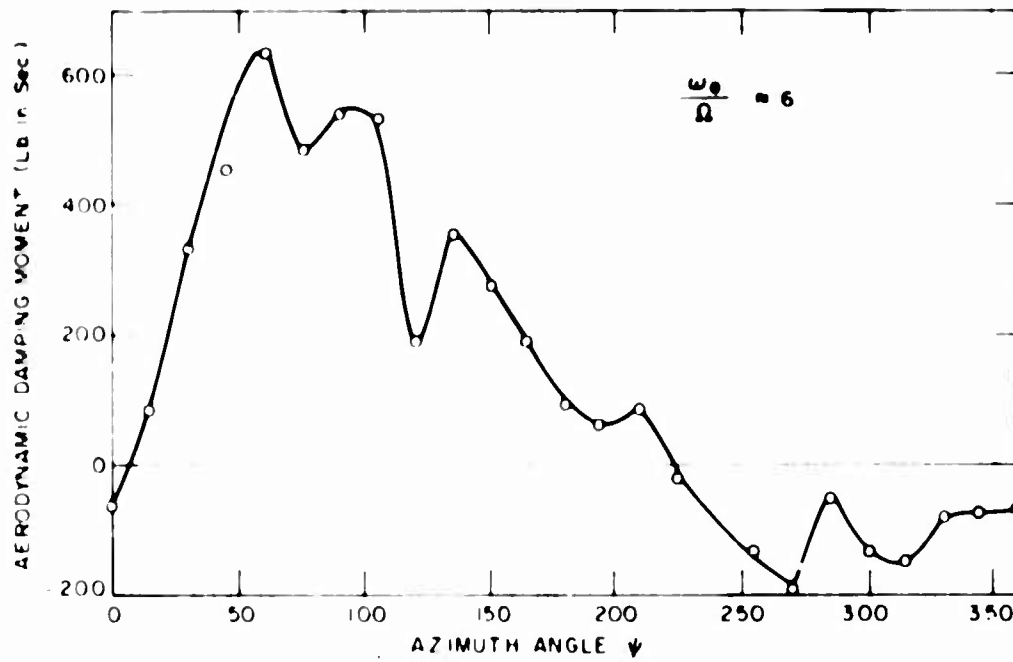
Fig 14 Net aerodynamic damping moment for fundamental pitching-torsion mode
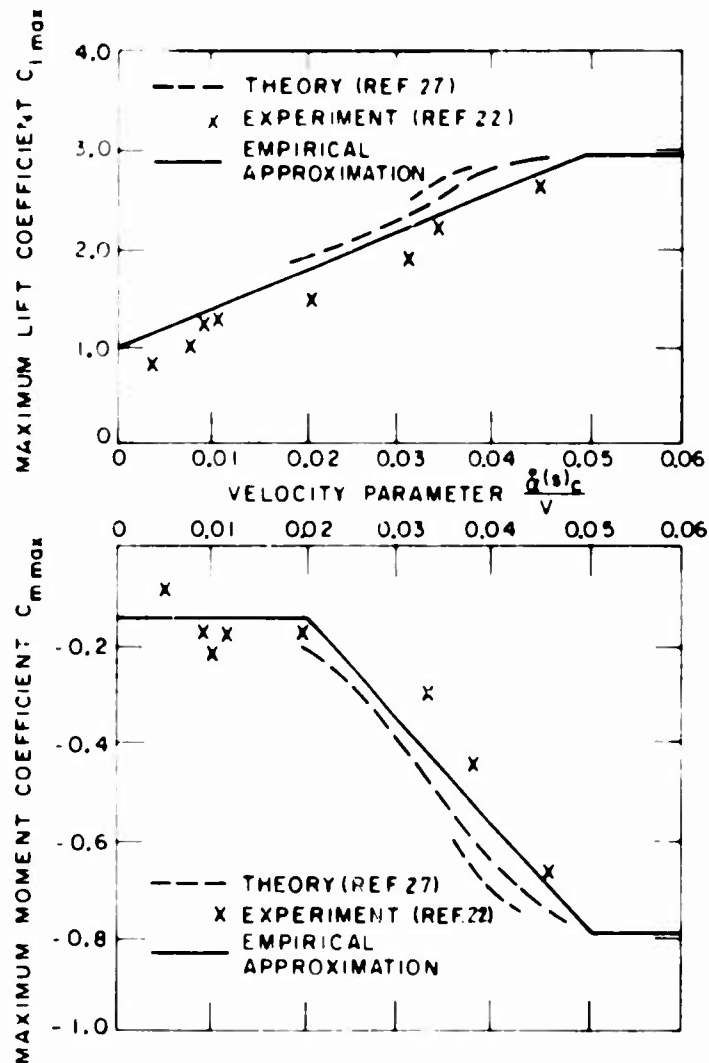
Fig 15 Maximum lift and moment coefficient versus rate of change of angle of attack
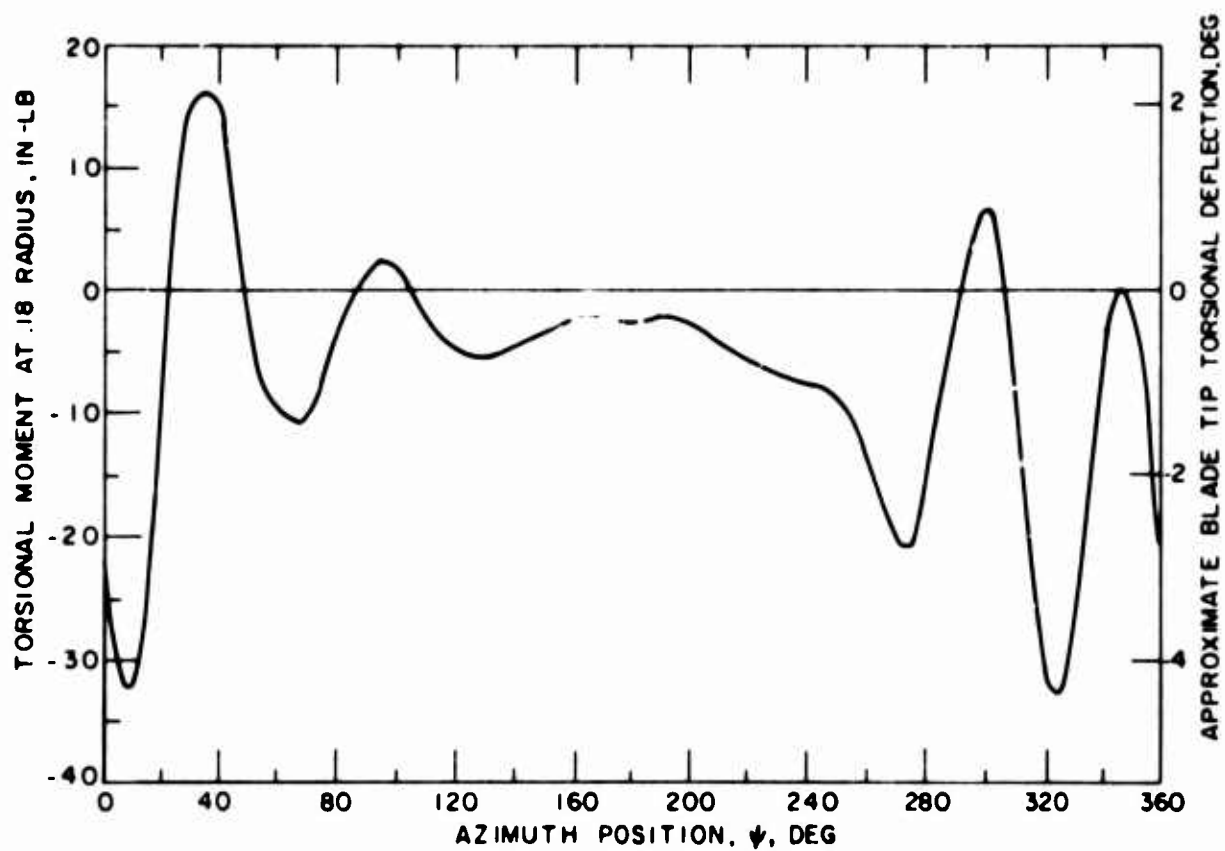
Fig.16 Blade response to stall flutter $\mu = .294$, $V = 120$ knots, $\theta_0 = 11°$, blade C.G at 25% chord

$\psi = 0°$

Fig 17   Blade angle of attack distribution for case of Figure 16, $\mu = .294$, $i = 0$, $\frac{c_T}{\sigma} = 0.11$

MANUAL ON AEROELASTICITY

VOLUME I   INTRODUCTORY SURVEY
            PART I
            STRUCTURAL ASPECTS

VOLUME II   PART II
            AERODYNAMIC ASPECTS

VOLUME III PART III
            PREDICTION OF AEROELASTIC PHENOMENA

VOLUME IV   PART IV
            EXPERIMENTAL METHODS

VOLUME V   PART V
            FACTUAL INFORMATION ON FLUTTER CHARACTERISTICS

VOLUME VI   PART VI
            COLLECTED TABLES AND GRAPHS

General Editor
R.Mazet

CONTENTS OF VOLUME I

CONTENTS OF VOLUME II

* The dates given relate to the acceptance of the manuscript by AGARD

CONTENTS OF VOLUME IV

CONTENTS OF VOLUME V

CONTENTS OF VOLUME VI

SUPPLEMENTS AND REVISIONS

Report No.573	G.Piazzoli	Aeroelastic Test Methods, Experimental Techniques	Published Dec. 1970
Report No.574	R.Dat	Bibliography of Documents Containing Numerical Data on Planar Lifting Surfaces	Published Aug. 1970
Report No.578	E.C.Pike	Manual on Aeroelasticity: Subject and Author Index	Published Jan. 1971
Conference Proceedings CP80 Part I		Symposium on Unsteady Aerodynamics for Aeroelastic Analysis of Interfering Surfaces	Published April 1971
Report No.583	D.L.Woodcock	A Comparison of Methods Used in Lifting Surface Theory	Published June 1971
Report No.592	H. G Küssner	A Comparison of Methods Used in Flutter Research	Published Aug. 1972
Report No.596	E.F.Baird and W.B.Clark	Recent Developments in Flight Flutter Testing in the United States	Published Dec. 1972
Report No.607	N.D.Ham	Helicopter Blade Flutter	Present report